Audio-magnetotelluric data in the Dragoon Mountains Roadless Area, Cochise County, Arizona

by

Michael J. Baer

and

Douglas P. Klein

Open-File Report 84-417

This report is preliminary and has not been edited and reviewed for conformity with U.S. Geological editorial standards.

STUDIES RELATED TO WILDERNESS

The Wilderness Act (Public Law 88-577, September 3, 1964) and related acts require the U.S. Geological Survey and the U.S. Bureau of Mines to survey certain areas on Federal lands to determine their mineral resource potential. Results must be made available to the public and be submitted to the President and Congress. This report presents the results of an audio-magnetotelluric survey of the Dragoon Mountains Roadless Area (03201) in the Colorado National Forest, Cochise County, Arizona. The Dragoon Mountain Roadless Area was classified as a further planning area during the Second Roadless Area Review and Evaluation (RARE II) by the U.S. Forest Service, January 1979.

Table of Contents

Appendices

Tables

Table of Contents (Continued)

Page

Figures

Introduction

Data from 10 audio-magnetotelluric (AMT) soundings (4.5-27,000 Hz) in the Dragoon Mountains of central Cochise County of southeastern Arizona (figs. 1 and 2) are described in this report. These ten soundings are spaced at intervals of approximately 5 km (3 mi) and provide a reconnaissance picture of the geoelectrical structure to interpretive depths of about 2 km (6,562 ft) to 10 km (32,808 ft) for stations overlying alluvial and mountainous areas respectively. These data were collected as part of the wilderness mineral evaluation program of the U.S. Geological Survey (USGS). Data presented in this report are in preliminary form. Interpretation of this data will be described in a separate report.

The AMT method consists of recording natural magnetic field variations and their corresponding induced electric fields in the Earth at discrete frequencies in the range of a few Hz to tens of kHz. The principles of the AMT method correspond to those of the magnetotelluric (MT) method (Cagniard, 1953, Vozoff, 1972, Vozoff and others, 1963) but the signals employed are at higher frequency and originate mainly from atmospheric electrical disturbances rather than from ionospheric or magnetospheric phenomena. Strangway and others (1973) have considered the potential and limitations of the AMT method in mineral exploration. Particular case histories of the AMT method in mineral and geothermal environments have been described by Strangway and Kozier, 1979, Hoover and others, 1976, and Hoover and Long, 1976.

The Dragoon Mountains Roadless Area has been subject to previous geological and geophysical descriptions which provide considerable detail on its geological setting and mineral potential (Drewes and Meyer, 1983, Klein, 1983). The Dragoon Mountains of central Cochise County are one group of northwest-trending mountains in southeastern Arizona (fig. 1). The foot of the range lies at elevations of 1,370 - 1,525 m (4,500 - 5,000 ft); the highest peak, Mt. Glenn, reaches 2,292 m (7,519 ft). The Dragoon Mountain Roadless Area, about 180 km^2 (70 mi^2) in size, covers most of the northwestern part of the range.

Gold and lead vein mineralization has been mined in the Golden Rule Mine area just beyond the north end of the area, and lesser deposits of base and precious metals, tungsten and beryllium occur within and fringing the central and southern portions of the Dragoon Mountains (Keith, 1969 a, b). Larger deposits of base and precious metals exist in the Johnson Camp and Tourquoise - Courtland-Gleeson mining areas about 8 km (5 mi) to the northwest and southeast of the mapped area respectively.

Data Acquisition and Processing

The USGS AMT system (Hoover and others, 1976, 1978, Hoover and Long, 1976) records in analog form two sets of orthogonal magnetic (H) and electric (E) field amplitudes for each of several frequency bands logarithmically spaced from 4.5 - 27,000 Hz. These data were collected in May 1980 using a receiver system that has two frequency dependent band-pass filters. The filters that were used consisted of one responding with a Q of 50, the other a slightly narrower Q of 100; the narrow pass being used for the frequencies in

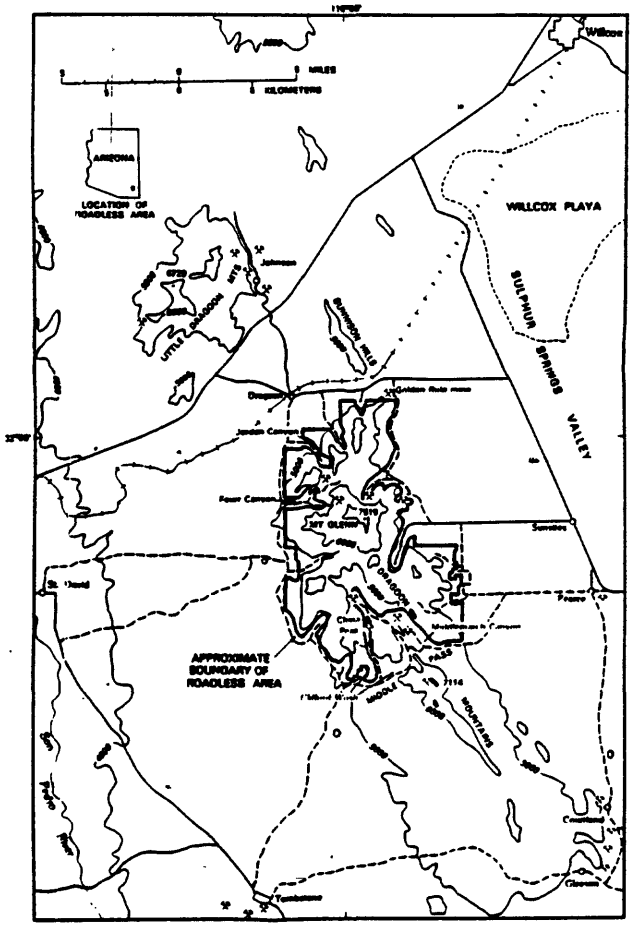

Index map showing the location of the Dragoon Mountains Roadless Area (03201).

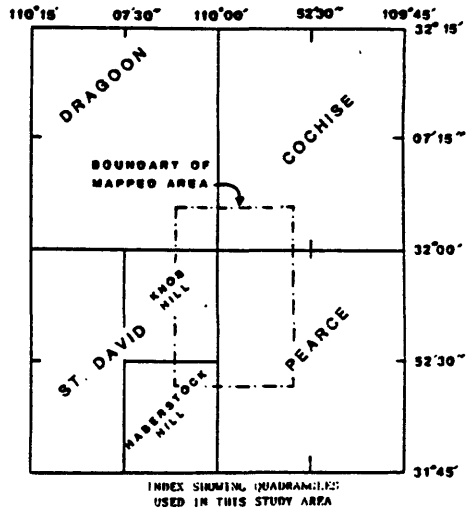

INDEX SHOWING QUADRANGLES USED IN THIS STUDY AREA

Figure 1 -- Map showing location of the Dragoon Mountain Roadless Area in central Cochise County, southeastern Arizona and the quadrangles used in this study area (from Klein, 1983).

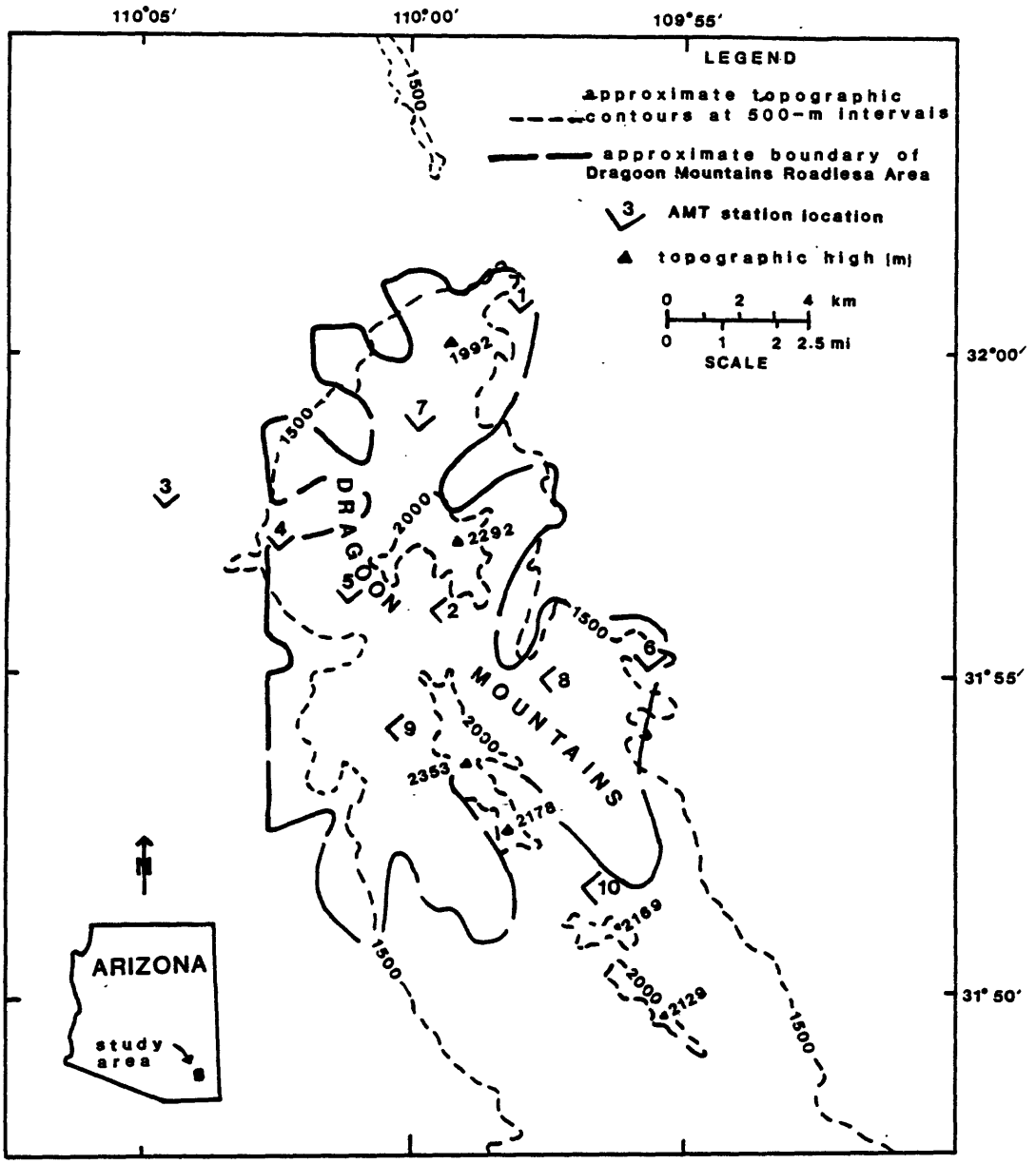

Figure 2 -- Map showing AMT station locations. The lines at each station indicate the orientation of the electric field dipoles (50 m; 164 ft). Elevations are in meters.

the 450-4,500 Hz range. Incoming magnetic signals were linearly multiplied by a factor of 80 in the range of 4.5 - 136 Hz and by 40 for frequencies of 450-27,000 Hz. The frequency of 270 Hz was used as the common frequency to change between these two gains. The actual gain used for 270 Hz was dependent on the signal strength and the operators' procedure while recording this frequency. The system additionally allows for the operator to independently contol the gains for the incoming E and H components. The system response factor (K), the magnetic coil gain, and the independent E and H gains for each of the band-pass frequencies recorded are listed in Appendix A.

The frequencies observed at each station (fig. 3) were all natural in origin except for the band between 10,000- to 20,000-Hz which partly utilizes navigation and communication signals.

Simultaneous peaks from each pair of orthogonal E-H records were digitized and reduced to scalar apparent resistivities (ohm-meters) using a hand calculator program as described by Klein and Baer (1983). The geographic E-field orientations chosen for this survey were northwest-southeast ($\rho_a$nw-se) and northeast-southwest ($\rho_a$ne-sw), and are assumed to be parallel or perpendicular to the major geological structures of the study area. The logarithmic mean of the data samples at each frequency, the number of samples scaled, the 95-percent confidence interval of the mean (as a percentage of a log cycle) and the gains used are tabulated in Appendix A. The confidence interval is a measure of the statistical consistency in the data but it does not reveal possible bias due to constant signal distortion. Such bias might be due to errors in system calibration, cultural electromagnetic interference, or signal polarization effects. Such a bias can be discovered only if independent data is available or if the bias is restricted to a limited number of frequencies. In the latter case, a bias may be apparent because part of the data does not conform to a consistant or physically plausible plot of apparent resistivity against frequency.

The reduced data were edited to reject data that were considered inconsistent with the trend of the sounding curve. The selection of data for rejection was performed independently on the $\rho_a$nw-se and $\rho_a$ne-sw curve each station. In as much as data editing is a subjective process, it is occasionally useful to iterate the editing and modelling, in order to test overall consistency among soundings. Note, for instance, that stations 1, 2, and 3 have two edited and modelled versions (see Appendices B and C). The alternate versions are denoted as 1A, 2A, and 3A respectively. These alternate versions are retained to illustrate possible uncertainties in the editing when a large initial scatter is present.

Figure 3 shows histograms of the percentage of data rejected for each frequency and thus indicates which observed frequencies were less reliable. Figure 4 shows three examples of complete soundings which illustrate the type of data rejected, and indicates the overall data quality. Those data that are within the dashed circles were discarded. The solid lines show a cubic polynomial fitted to the logarithmic mean of the edited data.

It can be seen from figure 3 that the frequencies in the 270-2,700 Hz range were rejected at about the 45-percent level compared to the data in the 4.5-136 Hz range which were rejected at about the 20- percent level. Two of the examples on figure 4, stations 4 and 9 are among the better data sets of

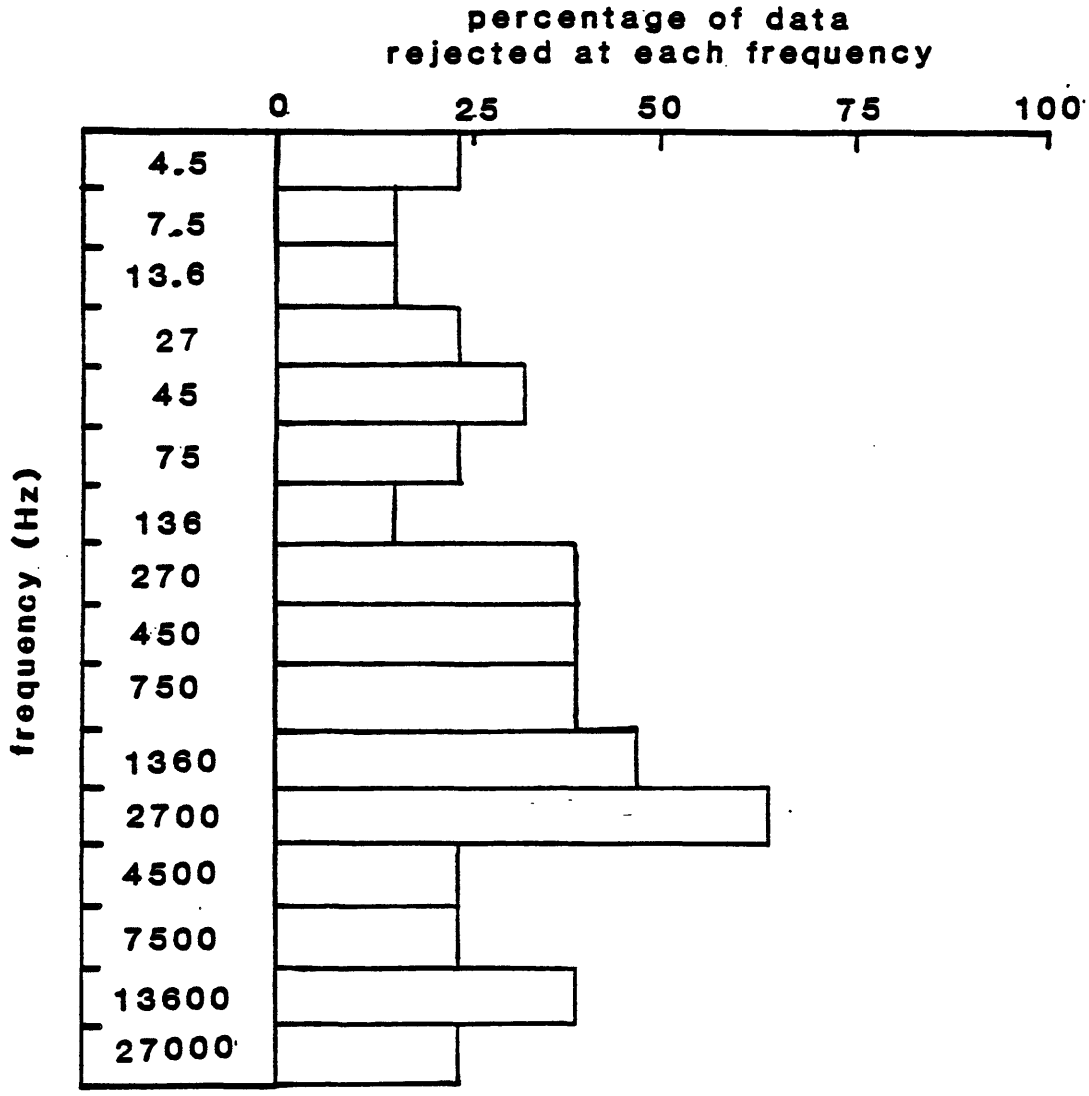

Figure 3 -- Histogram showing the percentage of AMT data rejected for each observed frequency. Note percentages are based on 13 stations which includes 1A, 2A, and 3A (see Appendix B).

this survey, whereas station 2 (fig. 4) illustrates data typically of the poorer soundings. Note in particular the variable apparent resistivities in the 450-2,700 Hz range for station 2. These values are attributed to insufficient signal strength during the recording period. The data rejected in the 4.5-450 Hz range, about 15- to 40-percent (fig. 3) is probably due to the survey being performed before the onset of the summer period when signal strength peaks because of increased thunderstorm activity.

An average sounding curve was estimated at each station by fitting a cubic polynomial to the logarithmic mean of the edited $\rho_a$nw-se and $\rho_a$ne-sw data. The polynomial fit provides a smooth approximation to the data, objectively filters out random noise, and provides a means to interpolate between gaps in the data (Klein and Baer, 1983). The resulting polynomial sounding curves, along with the edited data are plotted in Appendix B (see also fig. 4).

The data analysis is based upon a transformation of the smoothed data (cubic polynomial) to a resistivity-depth function using Bostick's method (Bostick, 1977, Bostick and others, 1977, Goldberg and Rostein, 1982). The results of this transformation were refined to better fit the smoothed data using one-dimensional forward modelling (Klein and Baer, 1983), restricting the relative modelled error to less than 0.20. The resulting models of resistivity-depth along with the smoothed apparent resistivities versus skin-depth are shown in Appendix C.

Table 1 presents parameters that summarize the overall characteristics of the present AMT data. Data consistency (smoothness) describes the signal/noise relationship among the data; this is based on the relative misfit beween the logarithmic average of the edited data (y_a, apparent resistivity) from the smoothed data (cubic polynomial, y_c). The percent relative error of a cubic polynomial fitted to the logarithmic mean of the edited data is given by

$$100 \times \left[\frac{1}{N} \sum_{i=1}^{N} (y_{a_i} - y_{c_i})^2 / y_{c_i}^2\right]^{1/2}$$

where the summation is with respect to the i=1, ..., N frequencies corresponding to those of the observed data. Percent modelled error is the relative misfit between apparent resistivity calculated for the layered Earth model (ρ_m) and the smoothed apparent resistivity data (ρ_a) and is given by

$$100 \times \left[\frac{1}{N} \sum_{i=1}^{N} (\rho_{m_i} - \rho_{a_i})^2 / \rho_{a_i}^2\right]^{1/2}$$

where the summation is with respect to i=1, ..., N frequencies corresponding to those of the observed data. The distortion factor (apparent anisotropy) describes the separation of the $\rho_a$nw-se and the $\rho_a$ne-sw sounding curves. The values listed refer to the mean value of the absolute logarithmic ratio as given by

$$D = \frac{1}{N} \sum_{i=1}^{N} \text{abs}[\log (\rho_a\text{nw-se}/\rho_a\text{ne-sw})]$$

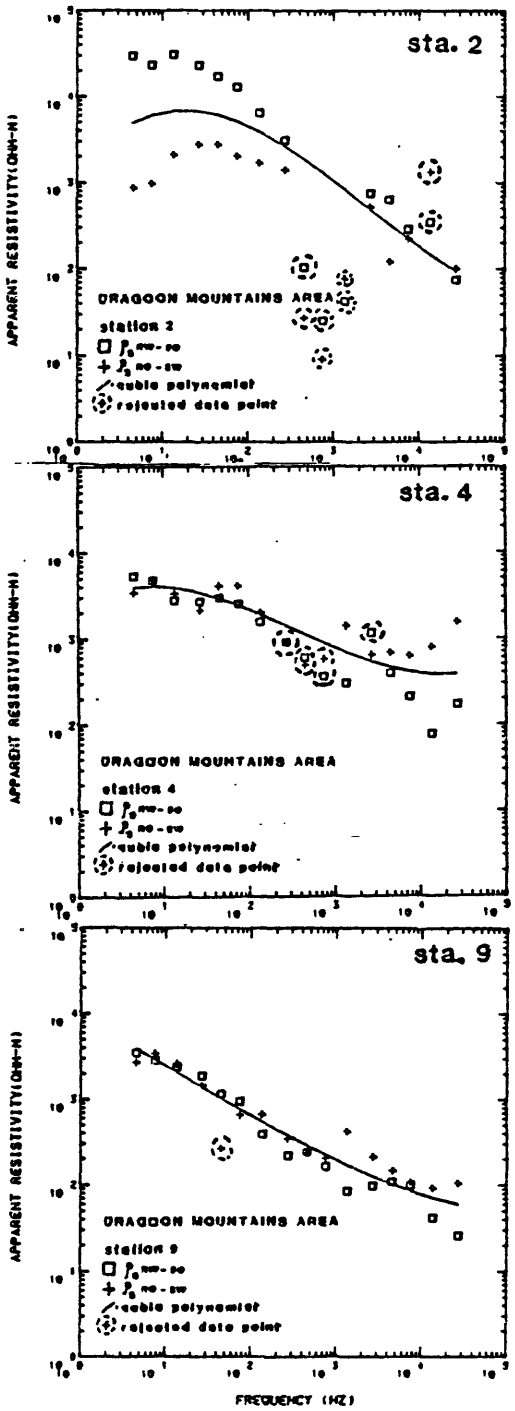

Figure 4 -- Examples of apparent resistivity-frequency curves. The cubic polynomial shown is based on the logarithmic mean of the saved data points. Station 2 illustrates one of the poorer data sets in the present survey, whereas stations 4 and 9 illustrate two of the better data sets obtained. See also Appendix B.

TABLE 1 -- Summary of data quality. Data consistency and modelled error are listed as percent relative error (misfit) between the smoothing function or forward model respectively.

Station	Data Consistency (Percent)	Percent Modelled Error	Distortion Factor (Apparent-Anisotropy)	Directional Factor
1	4.4	14.0	0.37	-0.99 (nw-se)
1a	2.9	12.2	1.00	-1.00 (nw-se)
2	2.2	13.2	*	1.00 (ne-sw)
2a	2.3	15.4	0.72	0.97 (ne-sw)
3	5.7	14.0	0.21	0.35 (ne-sw)
3a	4.4	11.9	0.28	0.18 (ne-sw)
4	3.3	17.2	0.32	-0.86 (nw-se)
5	2.9	18.3	0.46	-1.00 (nw-se)
6	2.2	15.2	0.52	-1.00 (nw-se)
7	3.2	13.3	0.33	0.79 (ne-sw)
8	3.4	19.0	0.31	-0.84 (nw-se)
9	3.1	10.7	0.20	-0.75 (nw-se)
10	2.8	11.4	0.15	-0.53 (nw-se)

*all ρ_{nw-se} values discarded

where the summation is with respect to i=1, ..., N frequencies corresponding to those of the observed data. The directional factor is the signed mean logarithmic ratio of the two orthogonal components and describes the consistency of the shift between orthogonal curves; the sign indicates the predominant direction of lower apparent resistivity. The directional factor is given by

$$\frac{1}{N} \sum_{i=1}^{N} \log \left(\rho_a \text{nw-se} / \rho_a \text{nw-se}\right)/D$$

where D is the distortion factor given above and the summation is with respect to i=1, ..., N frequencies corresponding to those of the observed data. Note that the directional factor is positive or negative unity if there is no crossover of the curves and becomes smaller as the sign of the numerator is not constant. The direction of lower resistivity based on the directional factor is shown in figure 5.

Resistivity Patterns

The results of the AMT data analysis, based on one-dimensional modelling of the smoothed logarithmic mean of ρ_a nw-se and ρ_a ne-sw (Appendix C) are summarized on Table 2 and in figures 6-10. Table 2 shows the resistivity-depth (or thickness) parameters interpreted from the layered Earth modelling. These parameters are also shown along with the contour maps (figs. 6, 7, 8) of the smoothed mean apparent resistivities for frequencies that are thought to reflect lateral resistivity contrasts associated with each layer. Figures 9 and 10 show contoured cross-sections of resistivity based on the smooth one-dimensional inversion (Bostick, 1977). It should be noted that for stations 1, 2, and 3 where alternate models are presented, the actual modelled data used to produce figures 6-10 consisted of 1, 2, and 3. Models 1A, 2A, and 3A were preliminarily tested and later rejected because of inconsistency to the overall geoelectrical pattern.

Figure 6 illustrates the apparent-resistivity distribution for the frequency of 7,500 Hz. The higher frequency AMT data (7,500 Hz and up) are probably detecting variations in near surface lithologies, weathering, and alterations. The interpreted resistivity and thickness of the layer is shown by each AMT station; the accompanying contours show the general pattern of lateral resistivity contrasts. On this map, as well as on figs. 7 and 8, the discrepancies between the interpreted resistivities and the apparent resistivities are due to the fact that the sounding curves (apparent resistivity-frequency curves) do not track modelled resistivities. The apparent resistivity at a particular frequency is a weighted mean function of the total geoelectric structure, where the weighting function peaks at a depth less than the skin-depth of that frequency and apparent resistivity (Weidelt, 1972, note also the curves of Appendix C).

Figure 6 indicates a surface layer, generally 3-10 m (10-66 ft) in thickness and of variable resistivity. The geological importance of the higher frequency AMT data is relatively low due to the fact that we are sensing only near surface conditions which could be presumably explored by alternate and more efficient methods. However, the higher frequency AMT data allows for a more complete definition of the sounding curve and thus more reliable modelling of the lower frequency data.

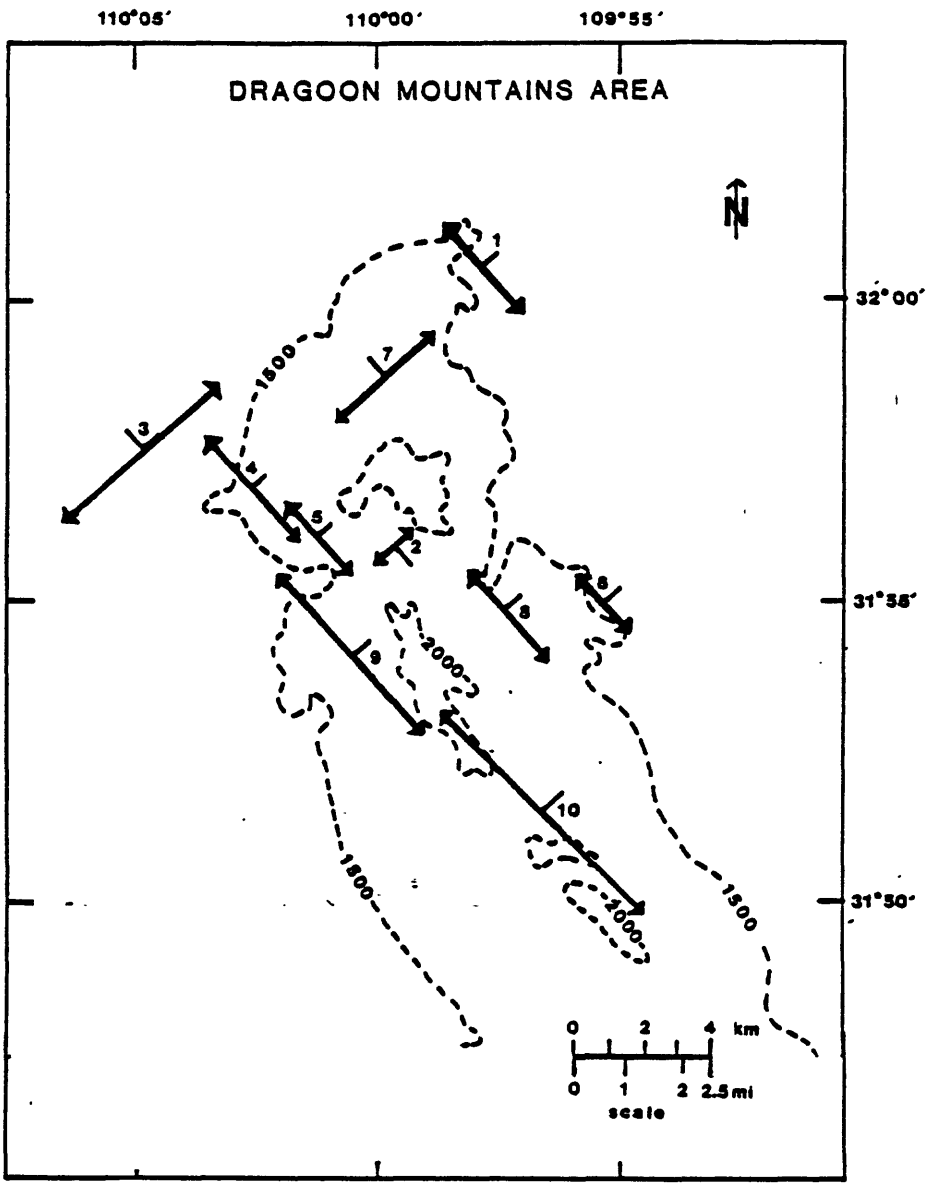

Figure 5 -- Map showing the direction of lower apparent resistivity at each station based on the apparent anisotropy parameter. The arrows point in the direction of minimum apparent resistivity and their lengths are inversely proportional to the distortional factor (i.e. the shorter length arrows are sensitive to lateral resistivity changes). See also Table 1.

TABLE 2 -- Interpretive summary of modelled layers. The three main horizons of contrasting resistivity parameters (modelled resistivity and depth or thickness, see Appendix C) as tabulated are also shown on figures 6, 7, and 8. The tabulated resistivities shown are rough logarithmic means over the intervals shown as thickness or depth.

	Surface Layer		Intermediate Layer		Deep Layer	
Station	Thickness (m)	Resistivity (ohm-m)	Depth Range (m)	Resistivity (ohm-m)	Depth Range (m)	Resistivity (ohm-m)
1	6	750	6-50	95	50-?	14000
1A	10	58	10-100	550	100-?	750
2	50	170	50-3000	4500	3000-?	275
2A	20	80	not indicated		20-?	8000
3	3	10	3-75	350	75-600	80*
3A	51	72	not indicated		51-?	153
4	15	5000	15-75	230	75-?	5000
5	10	2000	10-60	200	60-?	3000
6	10	700	10-100	90	100-?	2200
7	200	1800	not indicated		200-?	14000
8	100	125	not indicated		100-?	2200
9	20	55	20-200	300	200-?	5000
10	20	60	20-300	170	300-?	6000

*resistivity increases below 600 m.

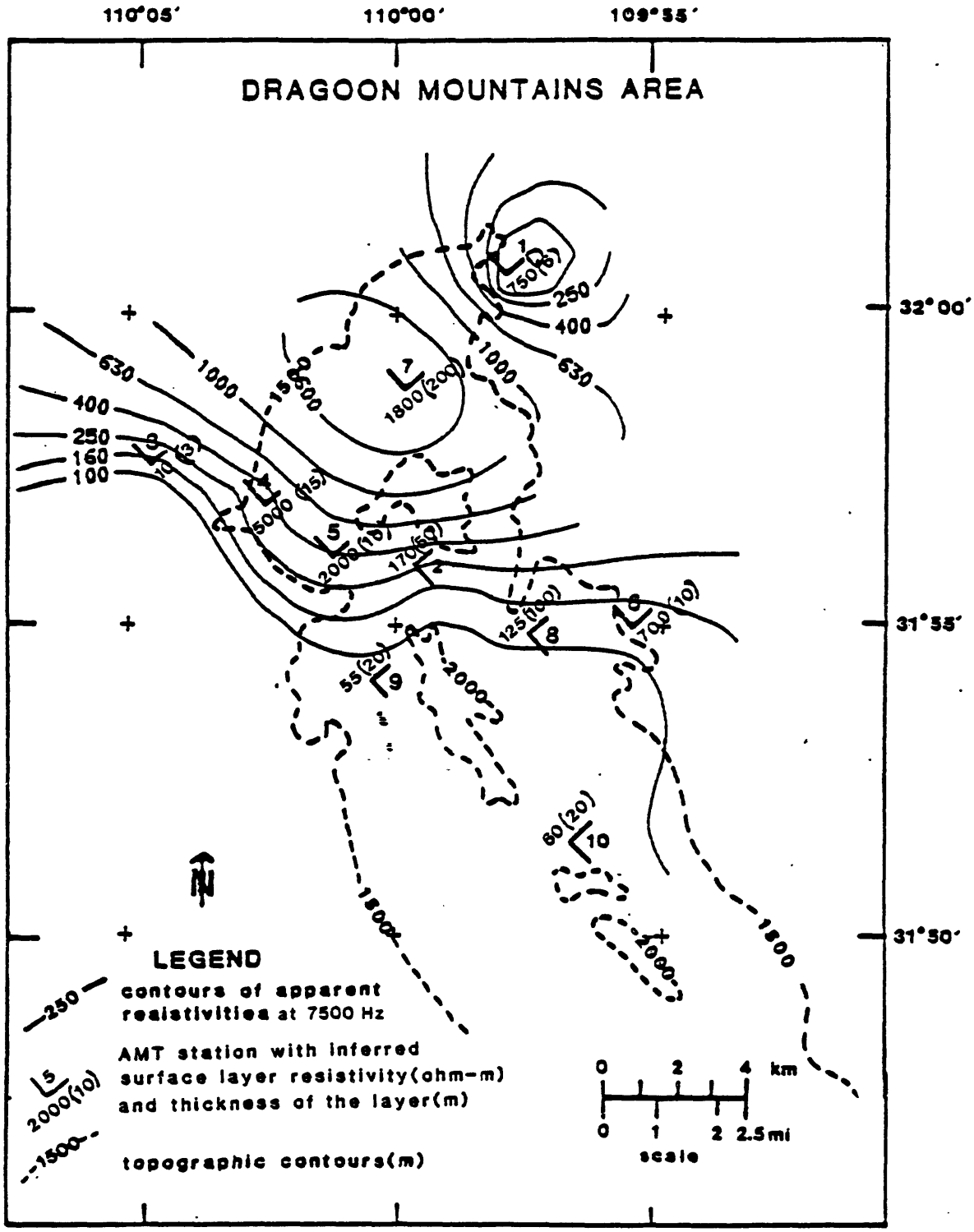

Figure 6 -- Map showing modelled surface-layer resistivity parameters and contoured apparent resistivity at the frequency 7,500 Hz. The contours are computer plotted, spaced at equal intervals of 5 divisions per decade on a logarithmic scale, and are based on a 1-km grid interval contoured by a USGS contour program (R. G. Godson, USGS, Denver, unpublished).

Figure 7 shows the interpreted resistivities and thickness of the intermediate-depth resistivity layer. These data are shown beside each station along with the contours of the smoothed apparent resistivity for the frequency of 270 Hz. This layer is typically 50-300 m (165 - 905 ft) in thickness. Two patterns of resistivity contrasts between the intermediate and the deep layers are apparent. Generally, however, the intermediate layer resistivity is low (90-300 ohm-m) as compared to the higher resistivities (2,200-14,000 ohm-m) of the deeper layer. Exceptions to this trend are where the intermediate layer is absent (stations 7 and 8, Appendix C), and where the "deep" layer indicates a decrease in resistivity (stations 2 and 3, Appendix C).

Figure 8 shows the interpreted depth and high resistivities of the deeper layer, along with contours of smoothed apparent resistivity at a frequency of 7.5 Hz. This high resistive (2200-1500 ohm-m) layer was detected at all stations and indicates a fundamental contrast with the overlying layers starting from 50-300 m (165-985 ft).

Figures 9 and 10 display two resistivity cross-sections of depth-resistivity based on a one-dimensional inversion of the apparent resistivity data. As previously described, the cubic-polynomial of the edited data (see Appendix B) was inverted to a resistivity-depth function by Bostick's method (1977). These data were then contoured using a USGS contour program (Ray Watts, 1983, USGS, Denver, Colorado, unpublished). The layered-Earth modelled resistivity for the deep layer are also shown; the top modelled resistivity is indicated in parenthesis at the approximate depth of the interface of the deep layer.

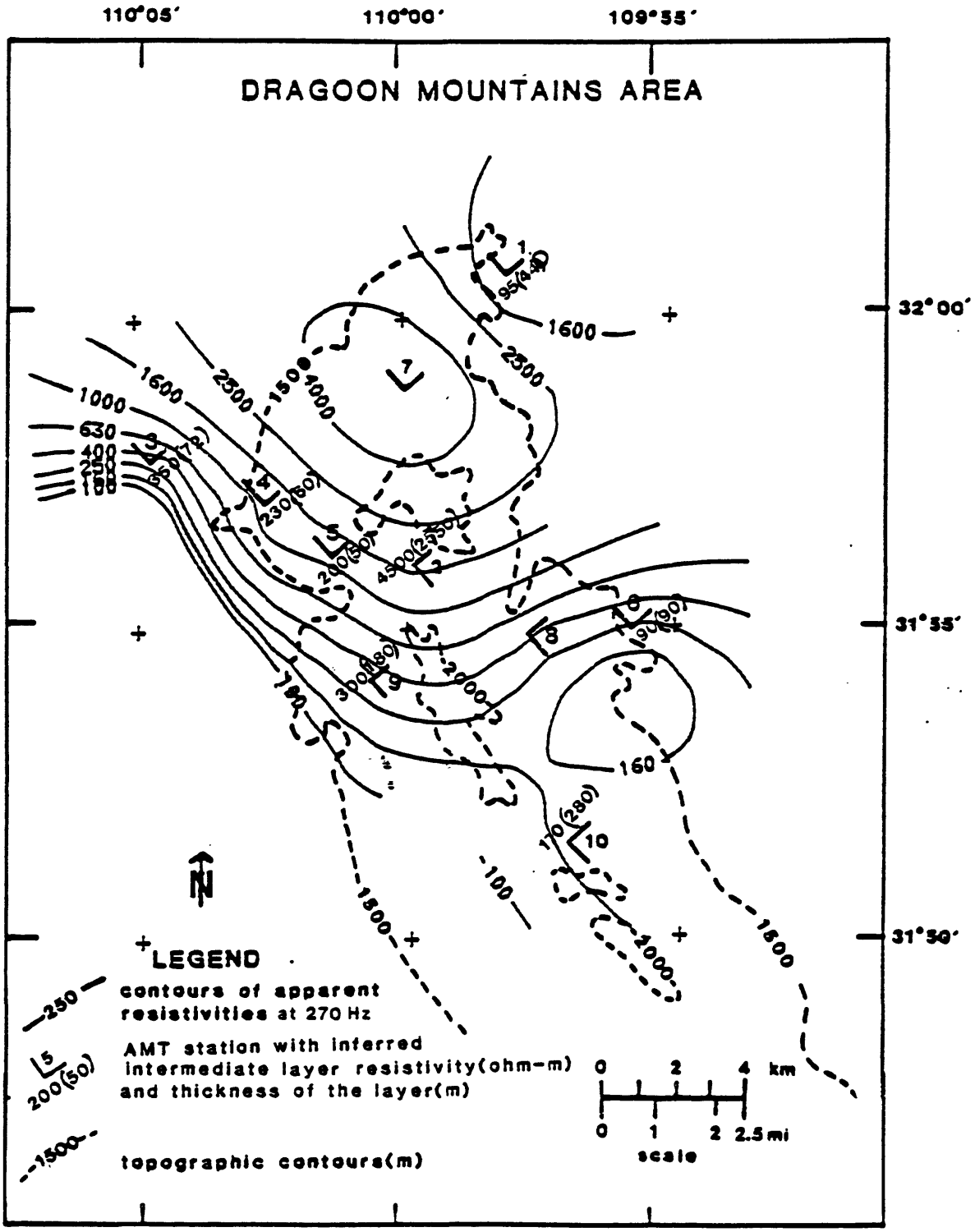

Figure 7 -- Map showing modelled intermediate conductive layer parameters and contoured apparent resistivity at the frequency 270 Hz. Note the intermediate layer was not detected at stations 7 and 8 (Table 2 and Appendix C).

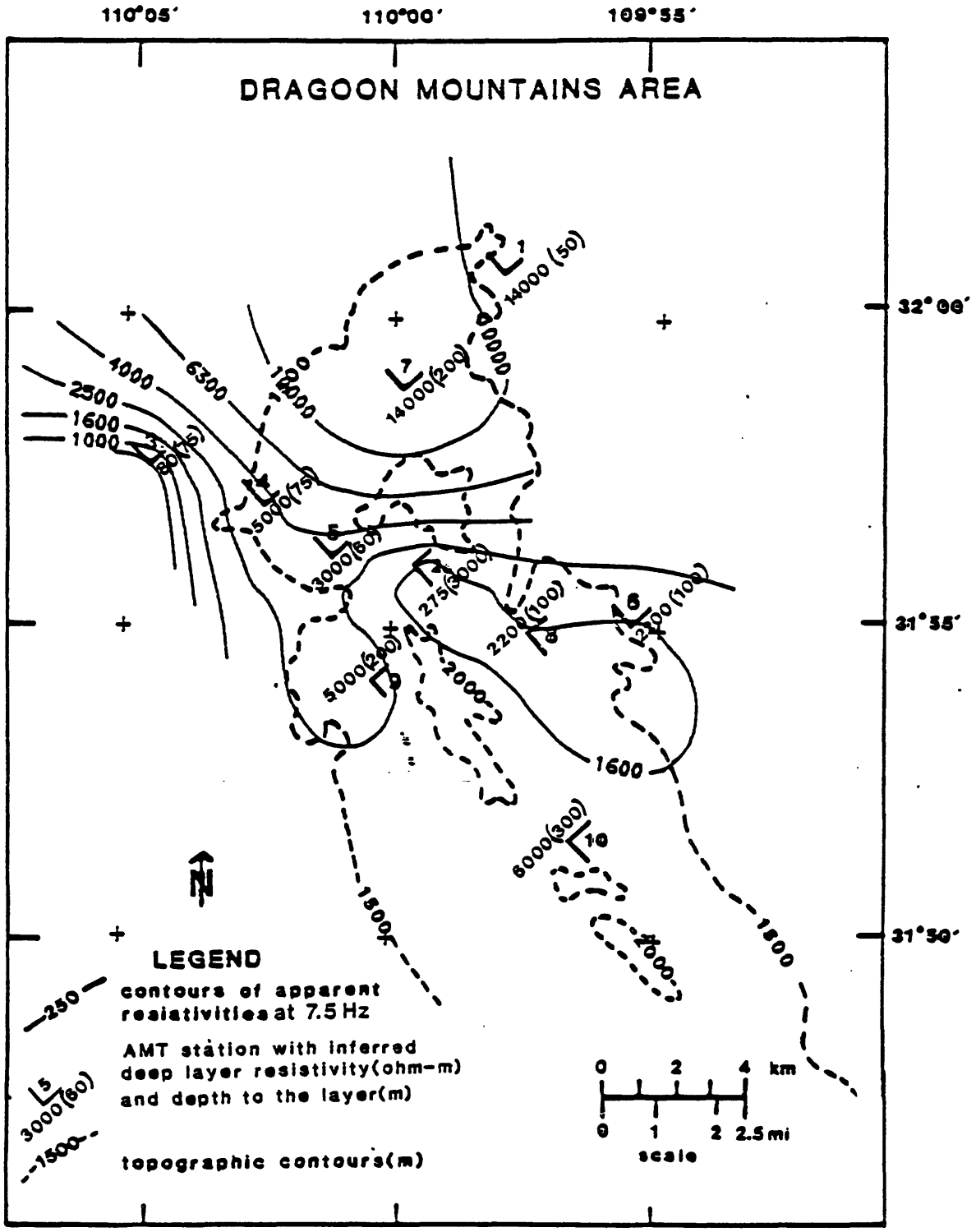

Figure 8 -- Map showing modelled deep resistive layer parameters and contoured apparent resistivity at the frequency 7.5 Hz. The contours are computer plotted, spaced at equal intervals of 5 divisions per decade on a logarithmic scale, and are based on a 1-km grid interval contoured by a USGS contour program (R. G. Godson, USGS, Denver, unpublished).

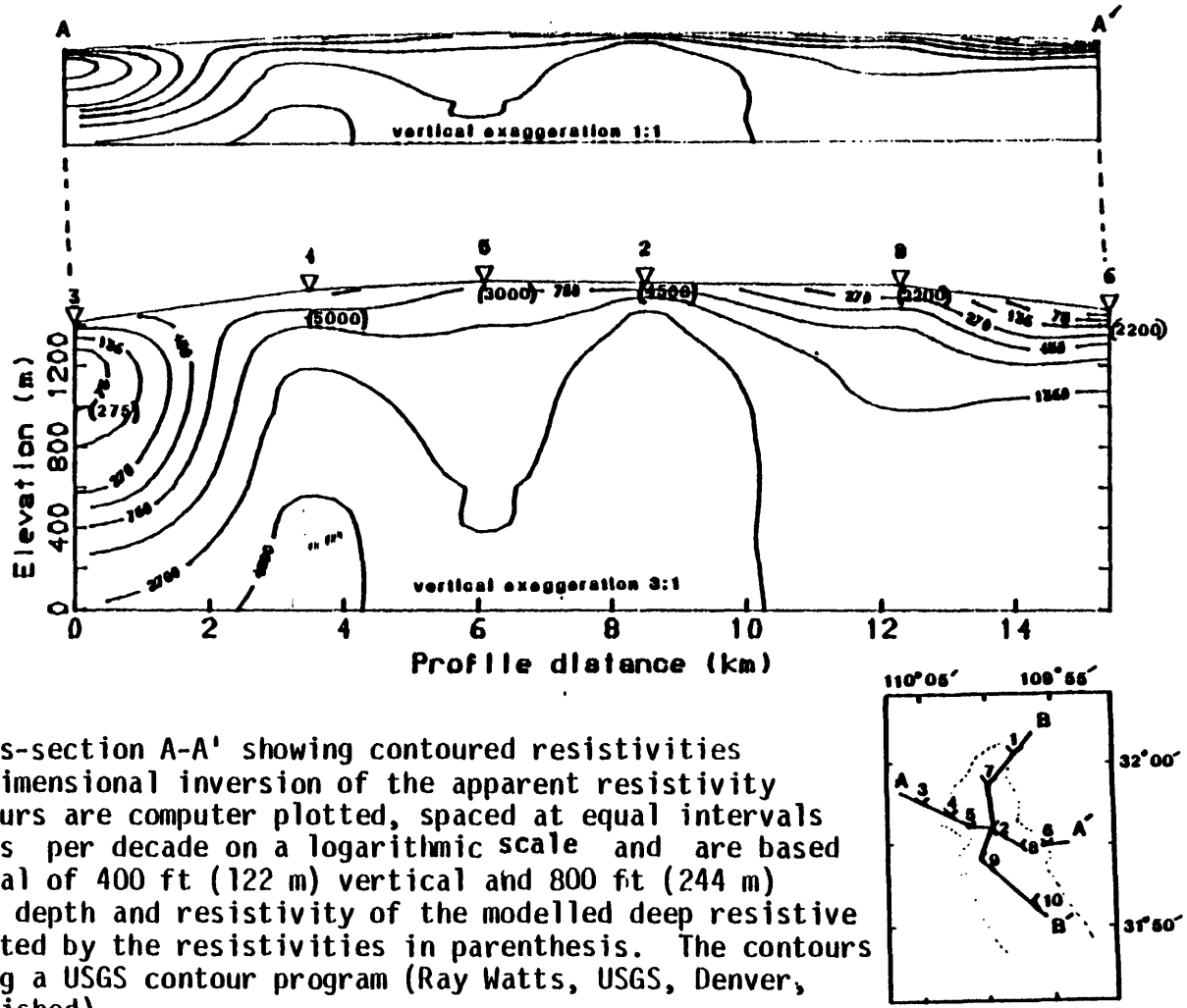

Figure 9 -- Geoelectric cross-section A-A' showing contoured resistivities based on a one-dimensional inversion of the apparent resistivity data. The contours are computer plotted, spaced at equal intervals of five divisions per decade on a logarithmic scale and are based on a grid interval of 400 ft (122 m) vertical and 800 ft (244 m) horizontal. The depth and resistivity of the modelled deep resistive layer are indicated by the resistivities in parenthesis. The contours are created using a USGS contour program (Ray Watts, USGS, Denver, Colorado, unpublished).

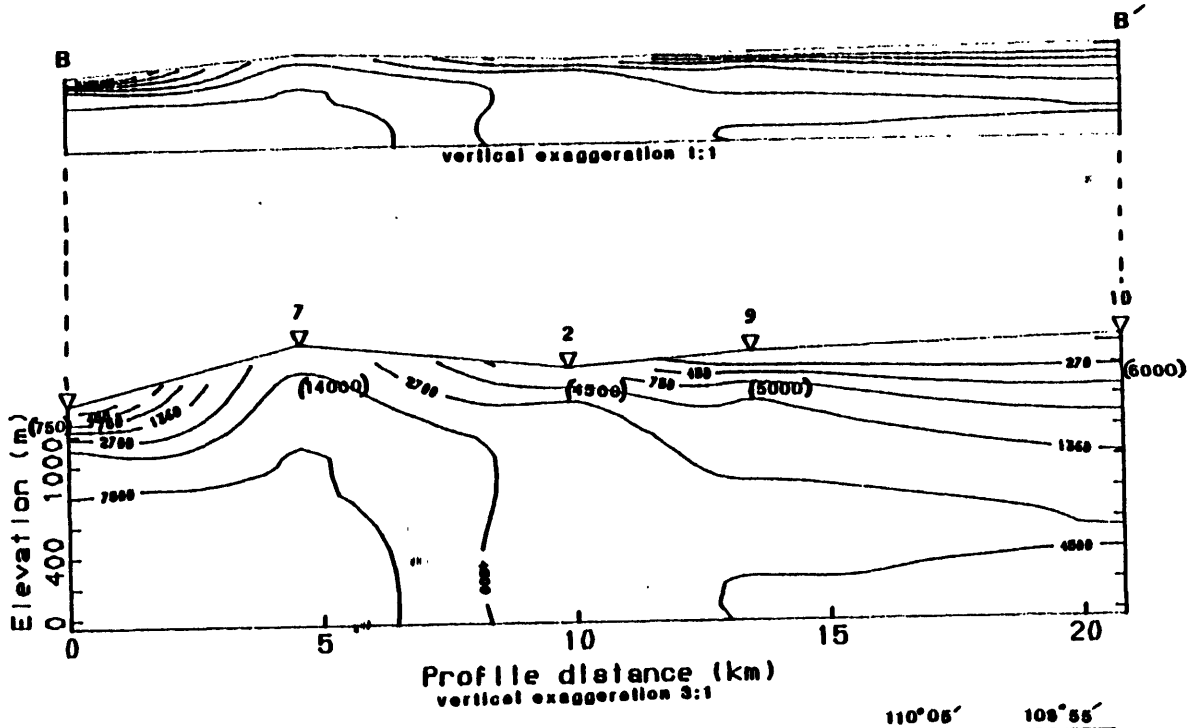

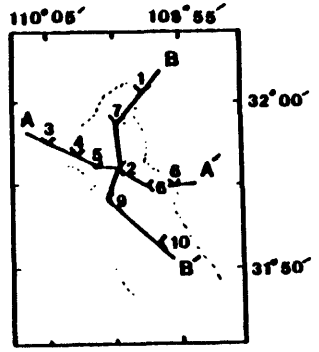

Figure 10 -- Geoelectric cross-section B-B' showing contoured resistivities based on a one-dimensional inversion of the apparent resistivity data. The contours are computer plotted, spaced at equal intervals of five divisions per decade on a logarithmic scale, and are based on a grid interval of 400 ft (122 m) vertical and 800 ft (244 m) horizontal. The depth and resistivity of the modelled deep resistive layer are indicated by the resistivity in parenthesis. The contours are created using a USGS contour program (Ray Watts, 1983, USGS, Denver, Colorado, unpublished).

Acknowledgements

Frances M. Boler assisted in the acquisition of the present data. Donald B. Hoover and Carl Long (USGS) provided valuable assistance in providing the equipment and assisting in survey preparation. The USGS AMT system was designed by Charlie Tippens, Jim Cooke, and others under the direction of D. B. Hoover.

References

Bostick, F. X., Jr., 1977, A simple almost exact method of MT analysis, "Workshop on evaluation of electrical methods in the geothermal environment (WEEMGE)", Snowbird, Utah, November 1976: University of Utah Report - Geothermal Workshop, January, 1977, p. 175-177.

Bostick, F. X., Jr., Smith, H. W., and Boehl, J. E., 1977, A simplified one-dimensional magnetotelluric inversion method, Appendix I in Magnetotelluric and DC dipole-dipole soundings on northern Wisconsin, Austin, University of Texas, Final Technical Report May 15, 1977, prepared under contract N00014-76-C, 0484, Office Naval Research, and Grant GA-38827, National Science Foundation, 52 p.

Cagniard, L., 1953, Basic theory of the magnetotelluric method: Geophysics, v. 18, no. 3, p. 605-635.

Drewes, Harold, and Meyer, G. A., 1983, Geologic map of the Dragoon Mountains Roadless Area, Cochise County, Arizona: U.S. Geological Survey Mineral Investigations Field Studies Map MF-1521-A.

Goldberg, S., and Rotstein, Y., 1982, A simple form of presentation of magnetotelluric data using the Bostick transform: Geophysical Prospecting, v. 30, p. 211-216.

Hoover, D. B., Frischknecht, F. C., and Tippens, C. L., 1976, Audio-magnetotelluric sounding as a reconnaissance exploration technique in Long Valley, California: Journal of Geophysical Research, v. 81, no. 5, p. 801-809.

Hoover, D. B., and C. L. Long, 1976, Audio-magnetotelluric methods in reconnaissance geothermal exploration: Proceedins 2nd United Nations Symposium Development and Utilization Geothermal Resources, v. 2, p. 1059-1064.

Hoover, D. B., Long, C. L., and Senterfit, R. M., 1978, Some results from audio-magnetotelluric investigations in geothermal areas: Geophysics, v. 43, no. 7, p. 1501-1514.

Keith, S. B., 1969a, Map of known metallic mineral occurrences (excluding base and precious metals) in Arizona: Tucson, Arizona Bureau of Mines, scale 1:1,000,000.

_____1969b, Map of known nonferrous base and precious metal mineral occurrences in Arizona: Tucson, Arizona Bureau of Mines, scale 1:1,000,000.

Klein, Douglas P., 1983, Gravity and aeromagnetic anomalies in the Dragoon Mountains Roadless Area, Cochise County, Arizona: U.S. Geological Survey Mineral Investigations Field Studies Map MF-1521-C.

Klein and Baer, 1983, Geoelectric structures of the Gila-San Francisco Wilderness area, Graham and Greenlee Counties, Arizona from audio-magnetotelluric data: U.S. Geological Survey Open-file Report 83-815, 26 p.

Strangway, D. W., and Kozier, A., 1979, Audio-frequency magnetotelluric sounding - a case history at the Cavendish geophysical test range: Geophysics, v. 44, no. 8, p. 1429-1446.

Strangway, D. W., Swift, C. M., and Holmer, R. C., 1973, The application of audio-frequency magnetotellurics (AMT) to mineral exploration: Geophysics, v. 38, no. 6, p. 1159-1175.

Vozoff, K., 1972, The magnetotelluric method in the exploration of sedimentary basins: Geophysics, v. 37, no. 1, p. 98-141.

Vozoff, K., Hasegawa, H., and Ellis, R. M., 1963, Results and limitations of magnetotelluric surveys in simple geologic situations: Geophysics, v. 28, no. 5, Part I, p. 778-792.

Weidelt, Peter, 1972, The inverse problem of geomagnetic induction. Journal of Geophysics (Zeitschrift fur Geophysik), v. 38, p. 257-289.

Appendix A

Tabulation of basic apparent resistivity

Table A1 presents the instrument system response factors, K, for each of the band-passed frequencies recorded using an E-line of 50 m (160.04 ft). Note at 750 Hz two K-factors, subscripts a or b, were determined and are used as reference for tables A2-A11.

Tables A2-A11 present the following data for the stations described in this report:

STATION: Survey station number designation.

LAT-LONG: Location of each survey station given in degrees and minutes for the latitude and longitude of each station. Minutes are provided with decimal fractions.

E-LINE DIRECTION: Direction of the electric dipole lines, oriented in the geographic northwest-southeast (NW-SE) and northeast-southwest (NE-SW) for each station. The E-direction is is orthogonal to the measured magnetic field for each data set.

HZ: Frequency of observation in Hertz.

N: Number of simultaneous sample peaks digitized from each electric and magnetic field analog record for the purpose of computing apparent resistivity.

RESIS: Apparent resistivity: $\rho_a$nw-se for E-line direction nw-se and $\rho_a$ne-sw for E-line direction ne-sw.

ERR: 95-percent confidence internal in units of percent logarithmic cycle for each calculated apparent resistivity.

GAIN: Linear gain (G_L) of the E and H signals. The gains recorded in the field are in decibels (g_{db}) and have been converted to linear gains by $G_L = 10^{(g_{db}/20)}$. Note at 270 Hz the gains are subscript a or b, referring to the system response factor for a coil gain of 80:1 or 40:1 respectively (see also table A1).

Table A1 -- Tabulation of system response factors.

Frequency (Hz)	System response factors (K) for E-line directed		Coil Gain
	E_{nw-se}	E_{ne-sw}	
4.5	2.31	2.98	
7.5	4.51	4.77	
13.6	6.88	10.6	
27	13.4	19.4	80:1
45	14.8	23.4	
75	29.3	35.0	
136	49.5	74.5	
270	93.9_a, 26.1_b	134_a, 33.4_b	
450	56.1	62.6	
750	121	111	
1360	531	654	
2700	742	824	40:1
4500	88.4	89.4	
7500	31.6	24.1	
13600	20.4	58.3	
27000	1.92	10.6	

Note: The magnetic receiving coil used a constant gain of 80:1 for the frequency range of 4.5 - 136 Hz and 40:1 for the range from 450-27,000 Hz. The coil gain was changed at 270 Hz and either gain may be used at that frequency. The system response corresponding to the 80:1 and 40:1 coil gains at 270 Hz are subscripted a and b respectively, are referenced in Tables A2-A11.

AMT DATA

PROJECT: DRAGOONS

STATION: 1
LAT.,LONG.: 32 0.67, 109 58.06

E-LINE DIRECTION: NW-SE

HZ	N	RESIS	ERR	GAIN E, H
4.5	9	37.0	21.0	126,251
7.5	7	35.0	8.0	63,126
13.6	5	42.0	15.0	63,126
27.0	5	49.0	3.0	63,63
45.0	8	1220.0	5.0	4,32
75.0	8	1530.0	4.0	2,16
136.0	10	489.0	12.0	4,16
270.0	6	272.0	3.0	8,16 a
450.0	8	246.0	6.0	8,16
750.0	7	191.0	3.0	1,1
1360.0	10	176.0	12.0	4,4
2700.0	9	74.0	14.0	8,4
4500.0	9	238.0	7.0	8,16
7500.0	7	174.0	4.0	4,16
13600.0	6	76.0	4.0	4,8
27000.0	5	53.0	2.0	4,16

E-LINE DIRECTION: NE-SW

HZ	N	RESIS	ERR	GAIN E, H
4.5	7	8481.0	23.0	8,126
7.5	6	10028.0	18.0	4,126
13.6	7	5066.0	17.0	4,63
27.0	6	9669.0	14.0	4,63
45.0	5	10780.0	6.0	2,16
75.0	6	11145.0	26.0	2,16
136.0	5	3866.0	11.0	4,16
270.0	6	287.0	19.0	4,8
450.0	8	1628.0	15.0	2,8
750.0	7	484.0	13.0	2,2
1360.0	7	788.0	18.0	2,4
2700.0	8	352.0	22.0	4,8
4500.0	5	226.0	24.0	4,8
7500.0	7	175.0	12.0	4,16
13600.0	9	189.0	13.0	2,4
27000.0	5	206.0	2.0	2,8

AMT DATA

PROJECT: DRAGOONS

STATION: 2
LAT.,LONG.: 31 56.01, 109 59.62

E-LINE DIRECTION: NW-SE

HZ	N	RESIS	ERR	GAIN E, H
4.5	7	29641.0	15.0	4,251
7.5	8	22966.0	6.0	2,126
13.6	7	30575.0	7.0	2,126
27.0	6	22959.0	2.0	2,63
45.0	8	17046.0	3.0	1,32
75.0	7	12781.0	4.0	1,16
136.0	6	6443.0	2.0	2,16
270.0	11	3098.0	4.0	1,4 a
450.0	6	103.0	7.0	2,2
750.0	9	25.0	4.0	4,2
1360.0	7	42.0	11.0	8,4
2700.0	8	751.0	10.0	4,8
4500.0	7	631.0	5.0	4,16
7500.0	6	285.0	4.0	4,16
13600.0	7	346.0	3.0	4,16
27000.0	8	75.0	6.0	2,16

E-LINE DIRECTION: NE-SW

HZ	N	RESIS	ERR	GAIN E, H
4.5	9	873.0	19.0	16,126
7.5	8	976.0	13.0	8,126
13.6	7	2066.0	22.0	16,126
27.0	9	2814.0	24.0	16,126
45.0	5	2778.0	17.0	8,63
75.0	6	2017.0	25.0	8,63
136.0	7	1722.0	14.0	8,32
270.0	7	1395.0	22.0	8,16
450.0	5	27.0	15.0	8,4
750.0	7	9.0	7.0	8,2
1360.0	7	76.0	6.0	8,4
2700.0	7	519.0	6.0	8,8
4500.0	7	121.0	7.0	16,16
7500.0	7	218.0	6.0	8,32
13600.0	8	1329.0	7.0	4,16
27000.0	6	99.0	5.0	4,16

AMT DATA

PROJECT: DRAGOONS

STATION: 3
LAT.,LONG.: 31 57.55, 110 4.56

E-LINE DIRECTION: NW-SE					E-LINE DIRECTION: NE-SW				
HZ	N	RESIS	ERR	GAIN E, H	HZ	N	RESIS	ERR	GAIN E, H
4.5	10	482.0	27.0	16,251	4.5	5	30.0	8.0	16,63
7.5	5	154.0	11.0	16,126	7.5	8	203.0	8.0	16,63
13.6	7	137.0	15.0	32,126	13.6	4	190.0	6.0	16,63
27.0	7	50.0	8.0	16,32	27.0	6	73.0	11.0	16,32
45.0	7	45.0	6.0	8,16	45.0	5	58.0	5.0	16,16
75.0	6	56.0	4.0	8,16	75.0	6	64.0	7.0	8,16
136.0	6	81.0	3.0	4,8	136.0	7	106.0	9.0	8,8
270.0	7	96.0	5.0	8,16 a	270.0	6	106.0	4.0	8,16
450.0	6	120.0	5.0	4,4	450.0	5	100.0	3.0	4,4
750.0	9	141.0	15.0	2,2	750.0	6	77.0	3.0	4,2
1360.0	7	148.0	9.0	8,4	1360.0	8	330.0	10.0	4,4
2700.0	9	206.0	19.0	2,4	2700.0	6	219.0	6.0	8,4
4500.0	9	140.0	9.0	4,8	4500.0	7	96.0	8.0	8,8
7500.0	9	106.0	5.0	4,8	7500.0	6	41.0	5.0	8,16
13600.0	7	37.0	5.0	4,8	13600.0	5	68.0	3.0	4,4
27000.0	6	28.0	5.0	4,16	27000.0	6	137.0	3.0	4,8

AMT DATA

PROJECT: DRAGOONS

STATION: 4
LAT.,LONG.: 31 56.95, 110 2.48

E-LINE DIRECTION: NW-SE

HZ	N	RESIS	ERR	GAIN E, H
4.5	13	5301.0	18.0	2,126
7.5	7	4710.0	16.0	2,63
13.6	9	2758.0	12.0	2,32
27.0	10	2683.0	15.0	1,16
45.0	9	2962.0	13.0	1,16
75.0	6	2496.0	7.0	2,16
136.0	6	1549.0	11.0	2,8
270.0	6	894.0	15.0	1,4 a
450.0	8	593.0	13.0	1,4
750.0	10	356.0	14.0	2,2
1360.0	9	300.0	12.0	2,2
2700.0	12	1137.0	18.0	1,2
4500.0	9	390.0	5.0	2,4
7500.0	6	207.0	7.0	2,4
13600.0	6	77.0	5.0	2,4
27000.0	7	171.0	6.0	1,4

E-LINE DIRECTION: NE-SW

HZ	N	RESIS	ERR	GAIN E, H
4.5	10	3401.0	32.0	4,126
7.5	6	4791.0	18.0	4,126
13.6	7	3327.0	13.0	4,63
27.0	6	2134.0	13.0	4,32
45.0	5	4047.0	10.0	2,16
75.0	7	4087.0	8.0	2,16
136.0	6	1969.0	18.0	2,8
270.0	5	854.0	7.0	2,8
450.0	6	484.0	11.0	2,4
750.0	6	568.0	8.0	2,2
1360.0	5	1376.0	17.0	4,4
2700.0	7	634.0	11.0	2,4
4500.0	6	664.0	5.0	4,8
7500.0	5	619.0	6.0	2,8
13600.0	6	790.0	8.0	2,8
27000.0	4	1536.0	2.0	2,16

AMT DATA

PROJECT: DRAGOONS

STATION: 5
LAT.,LONG.: 31 56.12, 110 1.15

E-LINE DIRECTION: NW-SE

HZ	N	RESIS	ERR	GAIN E, H
4.5	9	1666.0	17.0	8,126
7.5	9	1444.0	13.0	8,126
13.6	8	1819.0	14.0	4,63
27.0	7	1843.0	8.0	4,63
45.0	7	1161.0	3.0	4,32
75.0	8	962.0	12.0	4,16
136.0	7	396.0	8.0	4,16
270.0	8	230.0	5.0	2,4 b
450.0	12	245.0	9.0	2,4
750.0	11	189.0	10.0	2,2
1360.0	13	401.0	11.0	2,2
2700.0	8	414.0	9.0	4,4
4500.0	5	291.0	3.0	4,4
7500.0	6	188.0	6.0	4,8
13600.0	7	75.0	6.0	4,8
27000.0	9	99.0	3.0	2,16

E-LINE DIRECTION: NE-SW

HZ	N	RESIS	ERR	GAIN E, H
4.5	8	7811.0	8.0	4,126
7.5	5	6613.0	8.0	4,63
13.6	4	3872.0	4.0	4,32
27.0	7	4006.0	7.0	4,32
45.0	6	3798.0	6.0	2,16
75.0	6	2684.0	7.0	2,16
136.0	5	2008.0	4.0	2,8
270.0	6	183.0	21.0	2,2
450.0	4	692.0	4.0	2,4
750.0	7	521.0	8.0	2,2
1360.0	5	1636.0	6.0	2,4
2700.0	5	1463.0	7.0	2,4
4500.0	5	670.0	3.0	2,4
7500.0	6	281.0	6.0	2,4
13600.0	5	318.0	2.0	2,4
27000.0	4	627.0	2.0	4,16

AMT DATA

PROJECT: DRAGOONS

STATION: 6
LAT.,LONG.: 31 55.14, 109 55.65

E-LINE DIRECTION: NW-SE

HZ	N	RESIS	ERR	GAIN E, H
4.5	8	755.0	12.0	16,251
7.5	8	483.0	13.0	16,126
13.6	8	537.0	7.0	8,63
27.0	8	410.0	10.0	8,32
45.0	7	335.0	6.0	4,16
75.0	6	230.0	4.0	4,8
136.0	7	181.0	2.0	4,8
270.0	4	127.0	9.0	2,4 a
450.0	12	158.0	10.0	2,4
750.0	11	72.0	17.0	2,2
1360.0	9	1395.0	16.0	2,4
2700.0	7	1115.0	8.0	2,4
4500.0	7	221.0	7.0	4,8
7500.0	7	119.0	2.0	4,8
13600.0	6	56.0	2.0	4,8
27000.0	5	252.0	4.0	2,16

E-LINE DIRECTION: NE-SW

HZ	N	RESIS	ERR	GAIN E, H
4.5	8	3286.0	19.0	8,126
7.5	4	4320.0	12.0	8,126
13.6	5	3600.0	2.0	8,63
27.0	9	1677.0	6.0	8,63
45.0	6	1959.0	4.0	4,32
75.0	7	1649.0	6.0	4,32
136.0	6	788.0	4.0	4,16
270.0	7	492.0	10.0	2,4
450.0	6	339.0	7.0	4,4
750.0	6	211.0	15.0	4,8
1360.0	7	949.0	13.0	4,4
2700.0	3	662.0	17.0	8,4
4500.0	6	355.0	10.0	2,4
7500.0	4	153.0	2.0	2,4
13600.0	4	198.0	2.0	2,4
27000.0	4	1513.0	6.0	2,16

AMT DATA

PROJECT: DRAGOONS

STATION: 7
LAT.,LONG.: 31 58.83, 109 59.93

E-LINE DIRECTION: Nw-SE

HZ	N	RESIS	ERR	GAIN E, H
4.5	6	35077.0	17.0	1,126
7.5	3	20134.0	10.0	1,63
13.6	7	27837.0	11.0	1,63
27.0	8	17890.0	11.0	1,32
45.0	7	17823.0	5.0	1,32
75.0	6	20175.0	6.0	1,16
136.0	9	6804.0	10.0	1,8
270.0	6	4432.0	4.0	1,4 a
450.0	5	3818.0	4.0	1,8
750.0	5	6087.0	18.0	1,4
1360.0	8	8783.0	11.0	1,4
2700.0	8	2008.0	8.0	1,2
4500.0	7	6434.0	9.0	1,8
7500.0	6	3214.0	8.0	1,8
13600.0	5	2104.0	5.0	1,8
27000.0	5	972.0	5.0	1,16

E-LINE DIRECTION: NE-SW

HZ	N	RESIS	ERR	GAIN E, H
4.5	5	6191.0	30.0	8,63
7.5	6	15365.0	20.0	2,63
13.6	5	7639.0	9.0	4,126
27.0	5	4623.0	20.0	2,63
45.0	4	4078.0	3.0	2,32
75.0	8	5484.0	11.0	2,32
136.0	6	7243.0	18.0	2,16
270.0	5	5524.0	12.0	2,8
450.0	7	2163.0	17.0	2,4
750.0	5	2324.0	5.0	2,2
1360.0	6	3490.0	5.0	2,4
2700.0	4	1686.0	5.0	2,2
4500.0	4	2354.0	9.0	2,8
7500.0	4	1618.0	4.0	2,8
13600.0	5	2476.0	4.0	1,4
27000.0	4	1995.0	7.0	1,8

AMT DATA

PROJECT: DRAGOONS

STATION: 8
LAT.,LONG.: 31 54.90, 109 57.64

E-LINE DIRECTION: NW-SE

HZ	N	RESIS	ERR	GAIN E, H
4.5	5	690.0	6.0	16,251
7.5	6	845.0	6.0	8,126
13.6	5	788.0	5.0	8,63
27.0	6	665.0	4.0	4,32
45.0	5	595.0	5.0	4,16
75.0	5	644.0	1.0	4,16
136.0	5	432.0	2.0	2,8
270.0	5	292.0	2.0	2,4 a
450.0	6	309.0	4.0	2,4
750.0	5	261.0	5.0	2,2
1360.0	4	152.0	5.0	4,4
2700.0	6	111.0	9.0	4,2
4500.0	5	151.0	7.0	4,4
7500.0	5	165.0	5.0	2,4
13600.0	4	74.0	2.0	2,4
27000.0	6	28.0	2.0	4,16

E-LINE DIRECTION: NE-SW

HZ	N	RESIS	ERR	GAIN E, H
4.5	5	3169.0	5.0	4,126
7.5	6	3479.0	6.0	8,126
13.6	6	2920.0	6.0	8,63
27.0	7	1816.0	8.0	4,63
45.0	6	1553.0	7.0	4,32
75.0	6	718.0	9.0	4,16
136.0	4	488.0	3.0	4,8
270.0	5	371.0	11.0	4,4
450.0	9	179.0	21.0	4,4
750.0	5	193.0	6.0	4,2
1360.0	7	255.0	6.0	4,2
2700.0	5	203.0	9.0	4,2
4500.0	4	223.0	5.0	4,8
7500.0	5	158.0	11.0	4,8
13600.0	3	111.0	16.0	4,4
27000.0	5	179.0	2.0	4,16

AMT DATA

PROJECT: DRAGOONS

STATION: 9
LAT.,LONG.: 31 54.19, 110 0.39

E-LINE DIRECTION: NW-SE

HZ	N	RESIS	ERR	GAIN E, H
4.5	8	3492.0	9.0	8,251
7.5	6	2837.0	6.0	8,251
13.6	7	2365.0	9.0	4,63
27.0	6	1870.0	4.0	2,32
45.0	5	1149.0	3.0	2,16
75.0	7	948.0	6.0	4,16
136.0	6	385.0	4.0	4,8
270.0	9	218.0	8.0	4,8 b
450.0	6	240.0	5.0	2,4
750.0	6	163.0	4.0	2,2
1360.0	6	85.0	3.0	8,4
2700.0	8	98.0	12.0	4,2
4500.0	7	108.0	7.0	4,4
7500.0	5	99.0	2.0	4,8
13600.0	5	42.0	3.0	4,4
27000.0	4	26.0	2.0	8,32

E-LINE DIRECTION: NE-SW

HZ	N	RESIS	ERR	GAIN E, H
4.5	5	2708.0	5.0	4,126
7.5	7	3439.0	8.0	4,126
13.6	5	2621.0	6.0	4,126
27.0	6	1450.0	8.0	4,32
45.0	6	263.0	10.0	2,8
75.0	6	655.0	5.0	4,16
136.0	8	667.0	12.0	4,16
270.0	7	342.0	6.0	2,8
450.0	5	231.0	4.0	2,4
750.0	6	203.0	6.0	2,2
1360.0	7	425.0	10.0	4,4
2700.0	6	210.0	7.0	4,2
4500.0	6	146.0	4.0	4,4
7500.0	6	108.0	3.0	4,8
13600.0	5	91.0	3.0	4,4
27000.0	4	104.0	2.0	8,16

AMT DATA

PROJECT: DRAGOONS

STATION: 10
LAT.,LONG.: 31 51.72, 109 56.81

E-LINE DIRECTION: NW-SE

HZ	N	RESIS	ERR	GAIN E, H	
4.5	9	2797.0	18.0	4,126	*
7.5	7	1966.0	8.0	8,126	*
13.6	6	837.0	11.0	8,63	*
27.0	8	612.0	8.0	4,16	*
45.0	7	383.0	13.0	4,16	*
75.0	6	191.0	7.0	4,16	*
136.0	6	281.0	8.0	4,8	*
270.0	6	166.0	9.0	2,4 a	*
450.0	7	169.0	10.0	4,4	*
750.0	8	98.0	10.0	4,2	*
1360.0	6	152.0	8.0	8,4	*
2700.0	6	92.0	11.0	8,4	*
4500.0	5	59.0	7.0	2,8	
7500.0	7	260.0	9.0	2,4	
13600.0	7	126.0	3.0	2,4	
27000.0	5	37.0	2.0	2,8	

E-LINE DIRECTION: NE-SW

HZ	N	RESIS	ERR	GAIN E, H
4.5	4	4.0	19.0	16,126
7.5	5	1816.0	10.0	8,126
13.6	5	1412.0	8.0	4,32
27.0	8	592.0	18.0	8,32
45.0	6	466.0	5.0	4,16
75.0	7	271.0	4.0	4,16
136.0	5	221.0	7.0	8,16
270.0	5	321.0	7.0	2,8
450.0	5	134.0	12.0	4,4
750.0	7	61.0	19.0	2,1
1360.0	7	132.0	9.0	8,4
2700.0	7	67.0	9.0	8,4
4500.0	5	131.0	2.0	4,8
7500.0	5	947.0	2.0	4,8
13600.0	5	860.0	3.0	4,16
27000.0	4	85.0	5.0	8,16

*Channel E_{nw-se} malfunctional and channel E_{ne-sw} was used to measure E_{nw-se}. The corresponding system response factors are listed under E_{ne-sw}, Table A1.

Appendix B

Graphs of edited data and their cubic-polynomial approximation

The cubic-polynomial, shown as the smooth solid line was fitted to the logarithmic mean of the $\rho_a$nw-se (squares) and $\rho_a$ne-sw (crosses) data. The plots are bilogarithmic apparent resistivity against frequency (Hz). Those data that are within the broken circle have been rejected because they do not show consistency to the general trends of the $\rho_a$nw-se or $\rho_a$ne-sw curves. Note that for stations 1, 2, and 3 alternate solutions have been presented in order to indicate that there may be more than one single solution that fits these data, especially when a large data scatter is present.

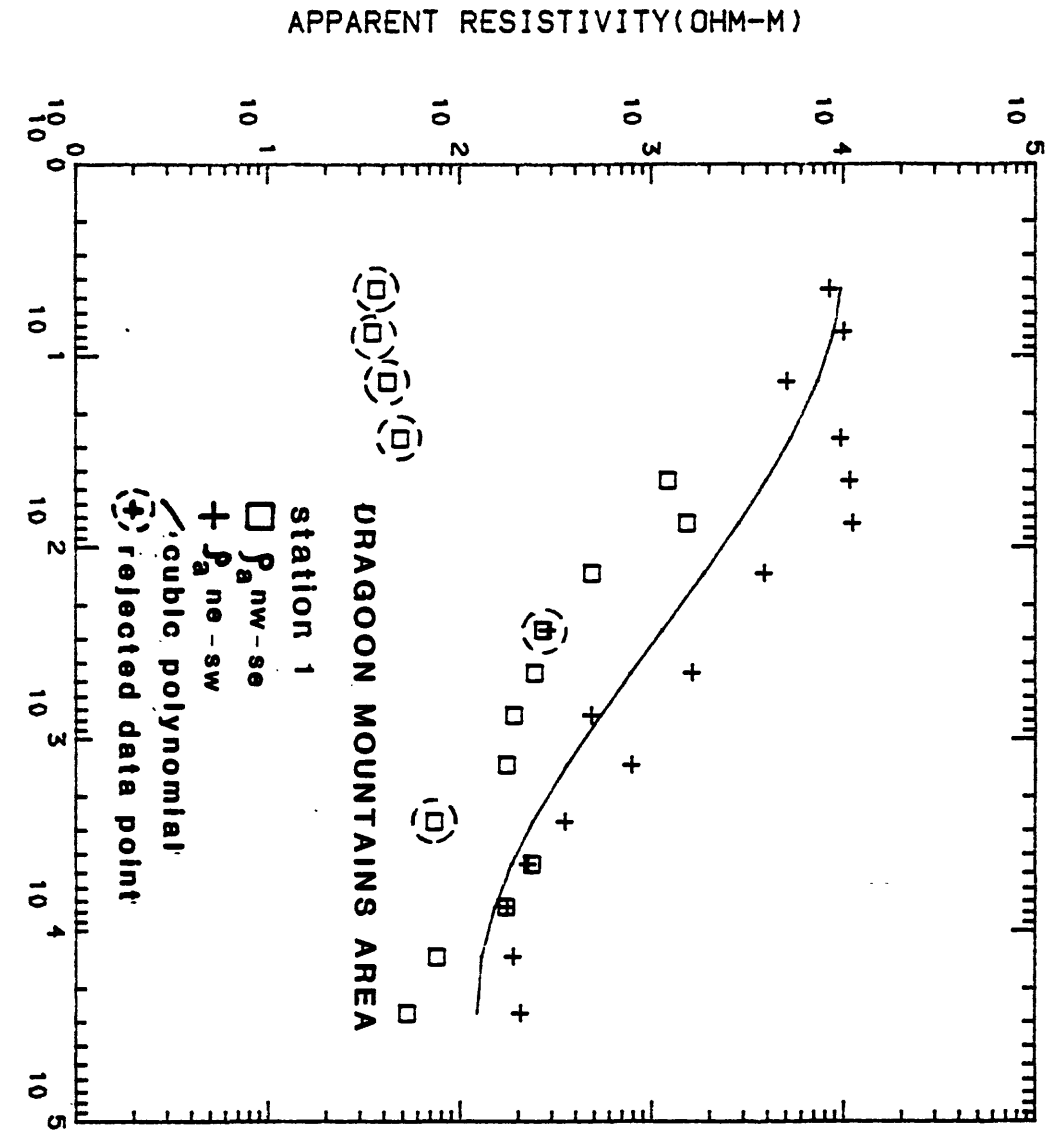
APPARENT RESISTIVITY(OHM-M)
FREQUENCY (HZ)
DRAGOON MOUNTAINS AREA
station 1
ρ_a nw-se
ρ_a ne-sw
cubic polynomial
selected data point

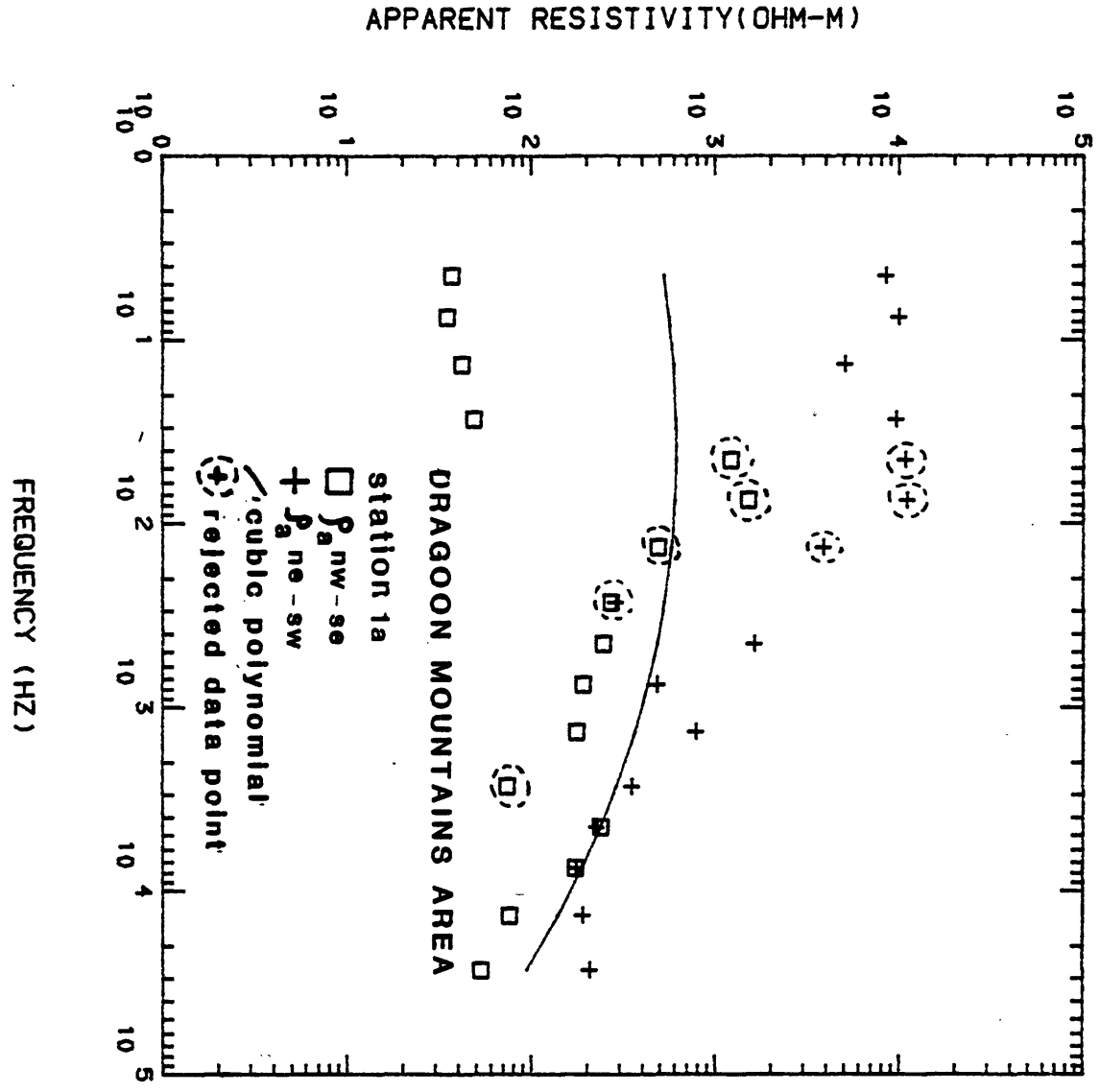
APPARENT RESISTIVITY(OHM-M)
FREQUENCY (HZ)
DRAGOON MOUNTAINS AREA
station 1a
ρ_a nw-se
ρ_a ne-sw
cubic polynomial
rejected data point

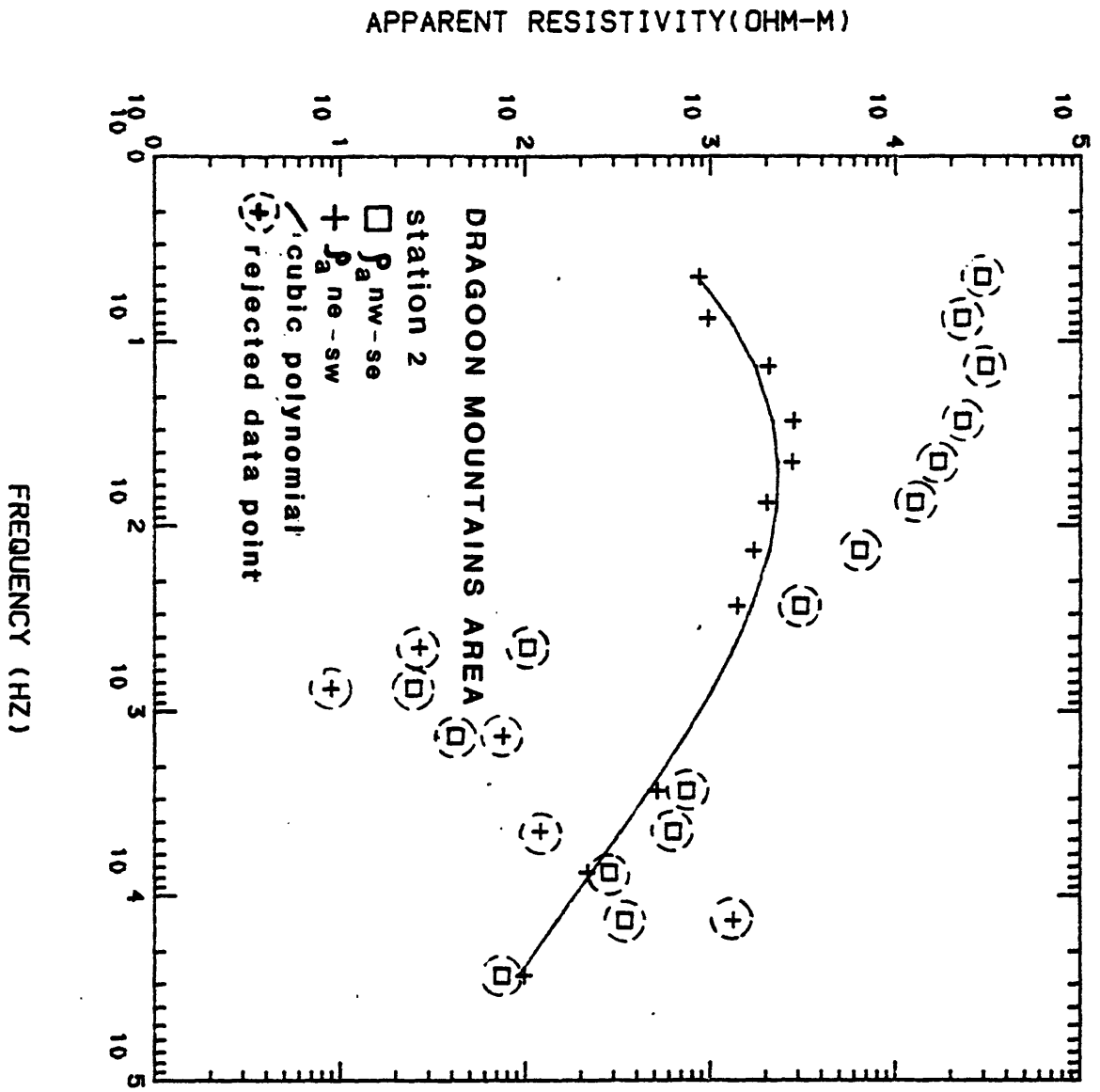
APPARENT RESISTIVITY(OHM-M)
FREQUENCY (HZ)
DRAGOON MOUNTAINS AREA
station 2
ρ_a nw-se
ρ_a ne-sw
cubic polynomial
rejected data point

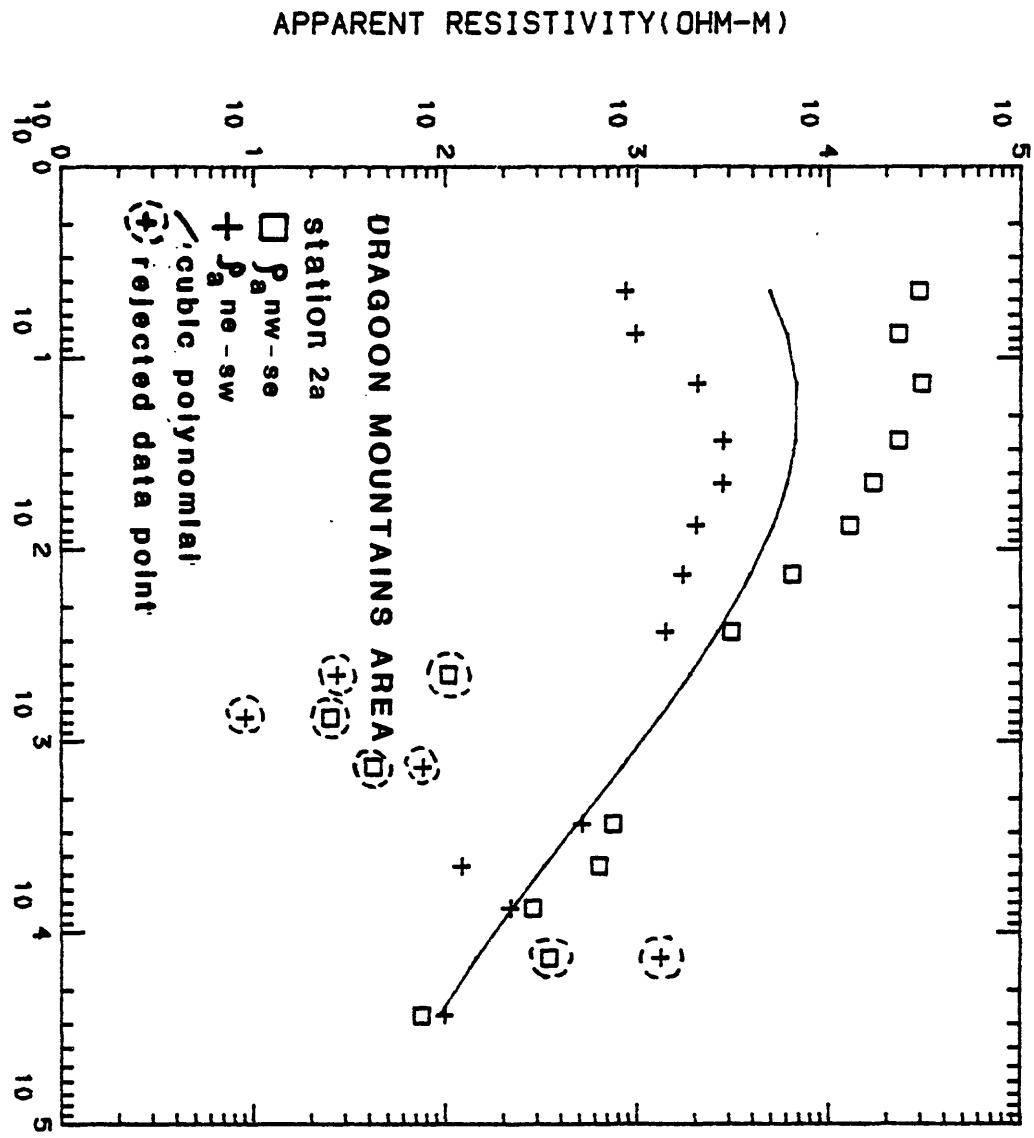
APPARENT RESISTIVITY(OHM-M)
DRAGOON MOUNTAINS AREA
station 2a
□ ρ_a nw-se
+ ρ_a ne-sw
cubic polynomial
(+) rejected data point
FREQUENCY (HZ)

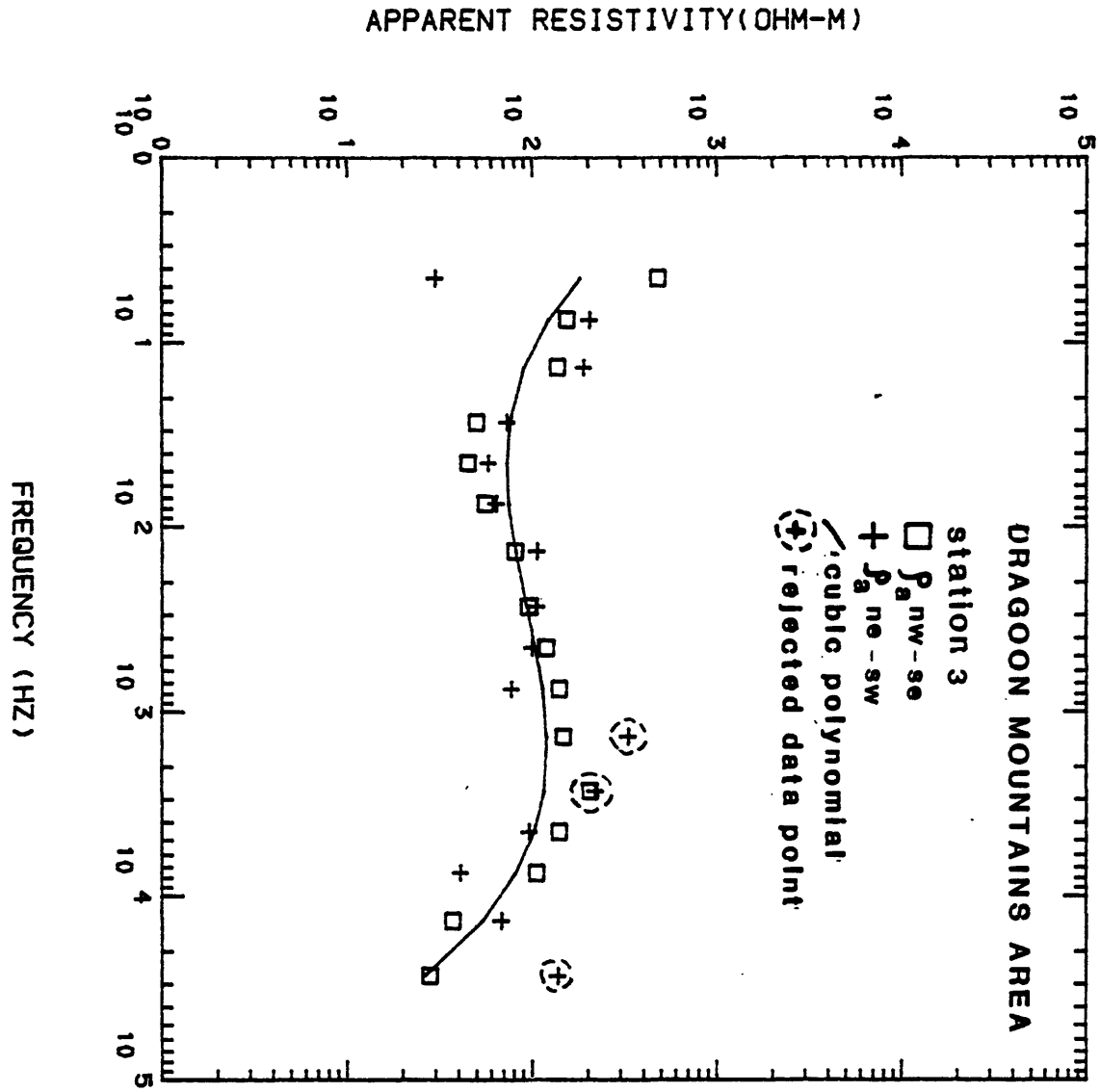
APPARENT RESISTIVITY(OHM-M)
DRAGOON MOUNTAINS AREA
station 3
□ ρ_a nw-se
+ ρ_a ne-sw
cubic polynomial
(+) rejected data point
FREQUENCY (HZ)

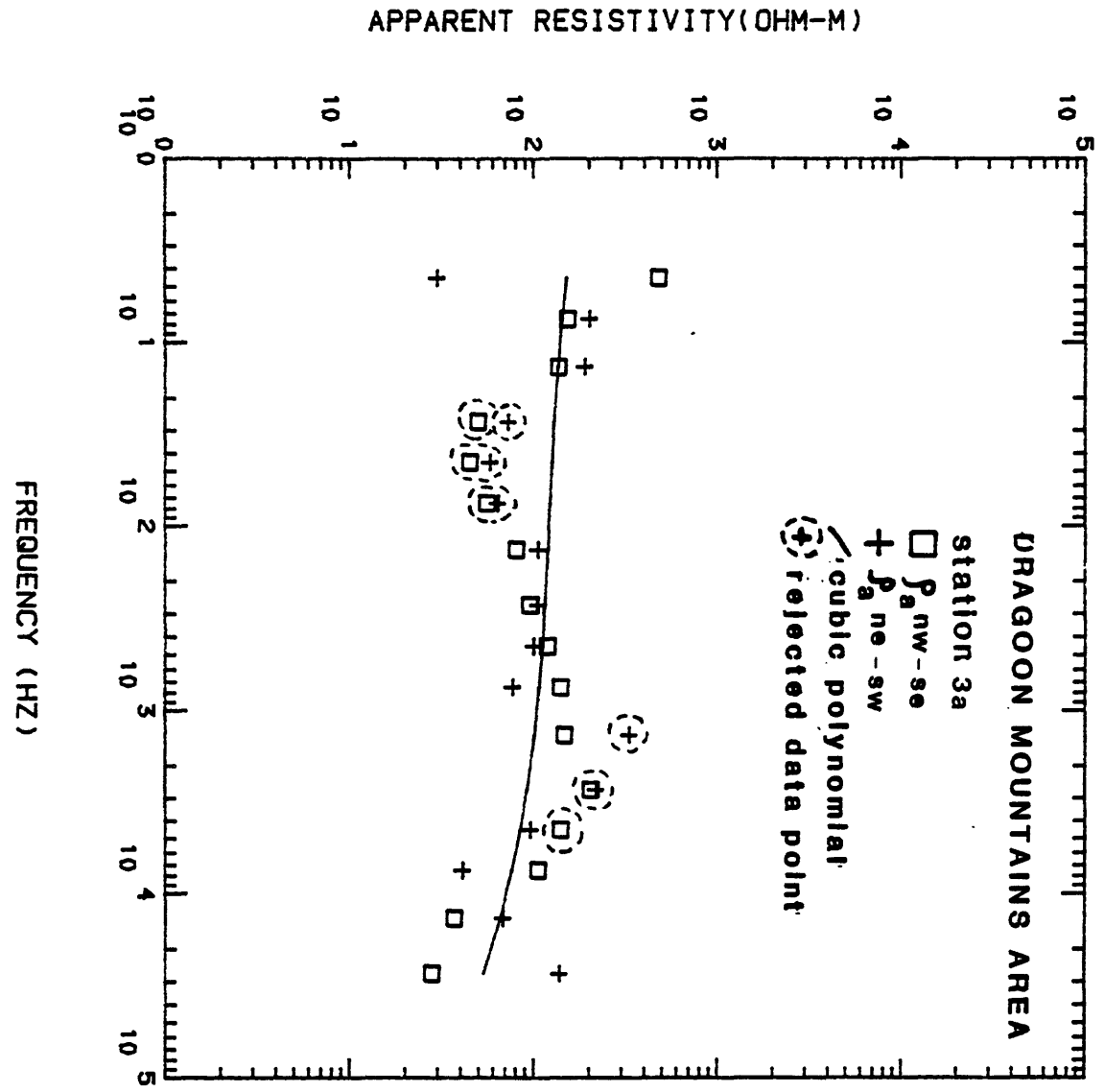
APPARENT RESISTIVITY(OHM-M)
FREQUENCY (HZ)
DRAGOON MOUNTAINS AREA
station 3a
□ ρ_a nw-se
+ ρ_a ne-sw
cubic polynomial
(+) rejected data point

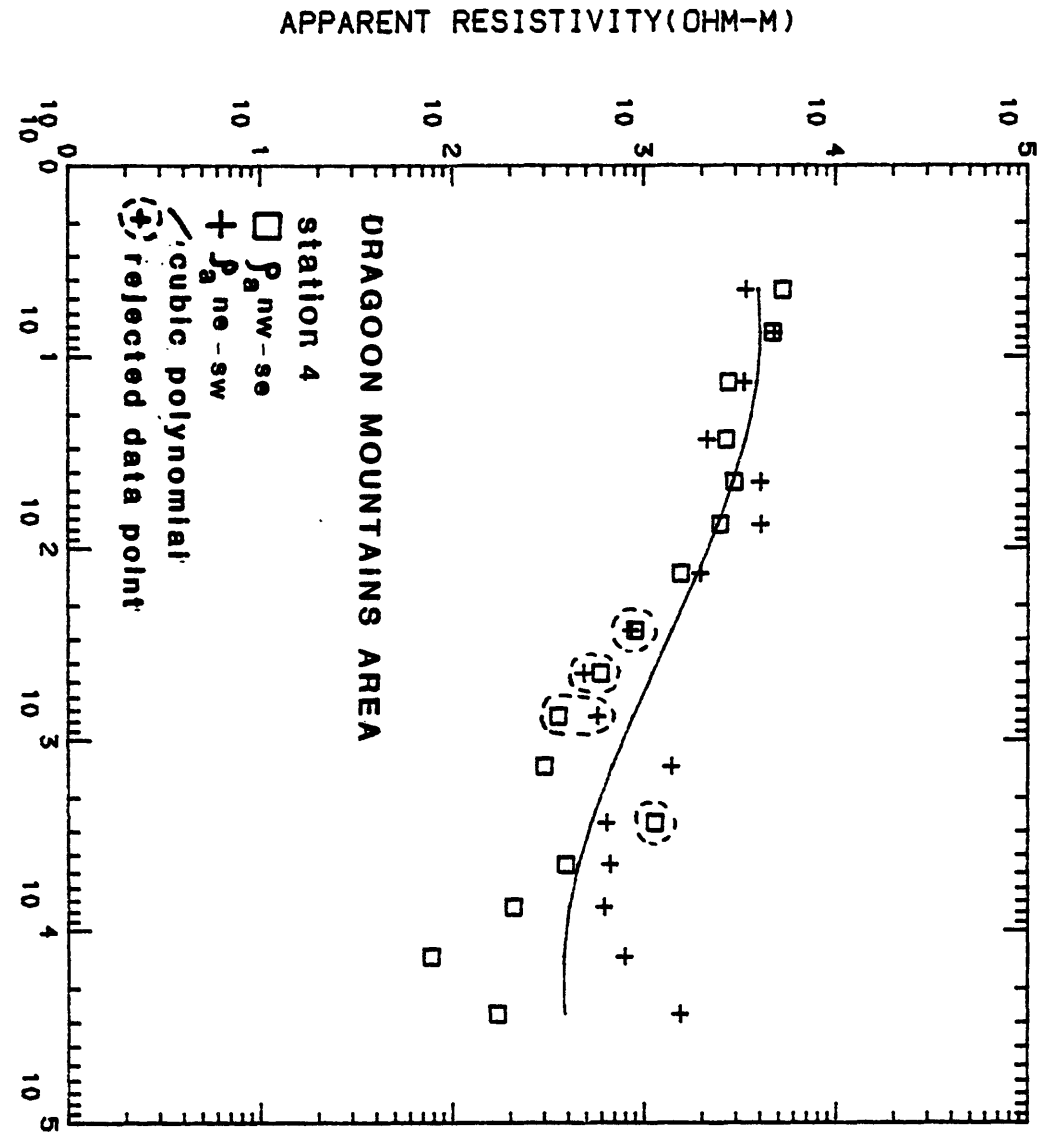
APPARENT RESISTIVITY(OHM-M)
DRAGOON MOUNTAINS AREA
station 4
□ ρ_a nw-se
+ ρ_a ne-sw
cubic polynomial
(+) rejected data point
FREQUENCY (HZ)

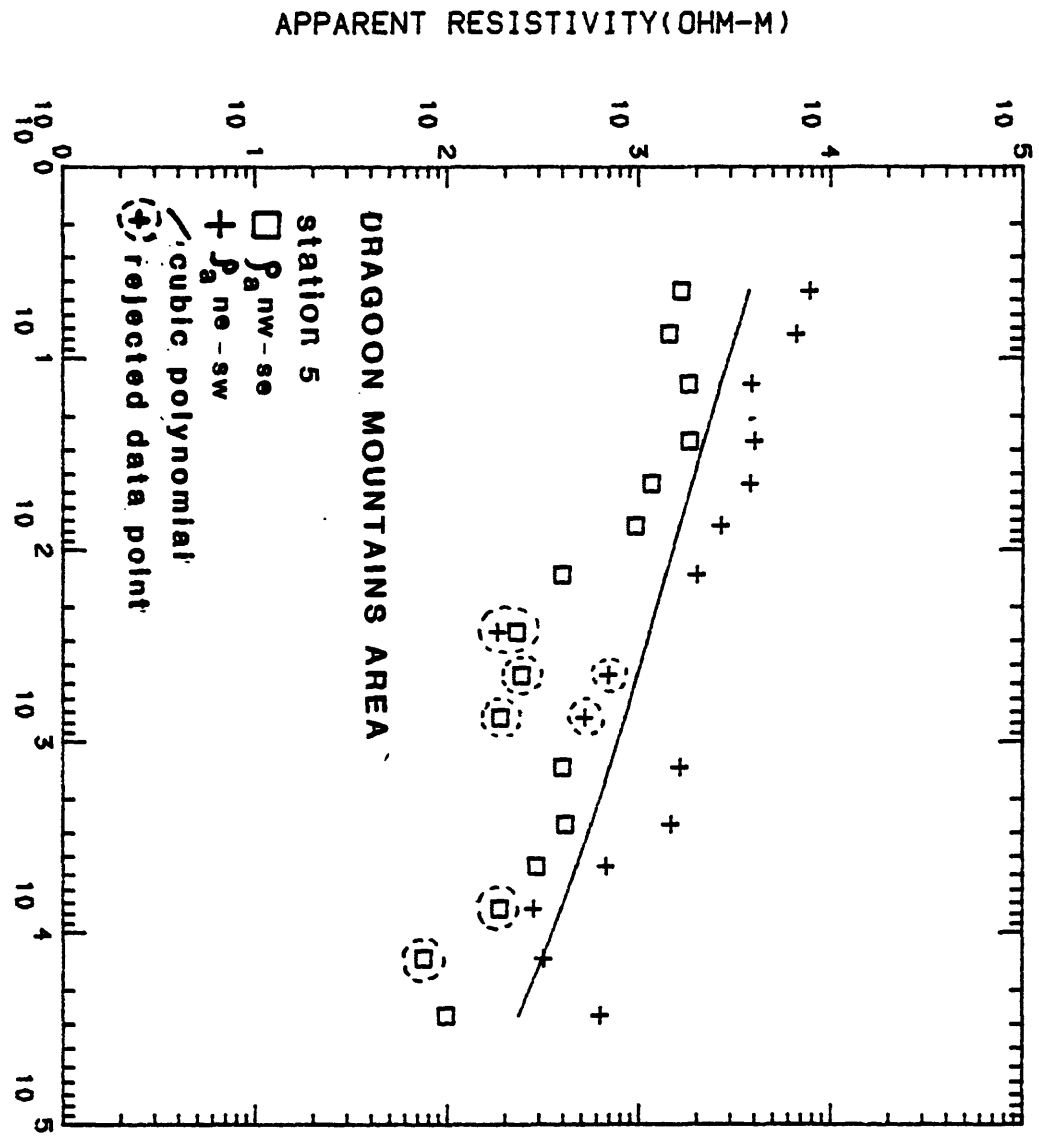
APPARENT RESISTIVITY(OHM-M)
FREQUENCY (HZ)
DRAGOON MOUNTAINS AREA
station 5
ρ_a nw-se
ρ_a ne-sw
cubic polynomial
rejected data point

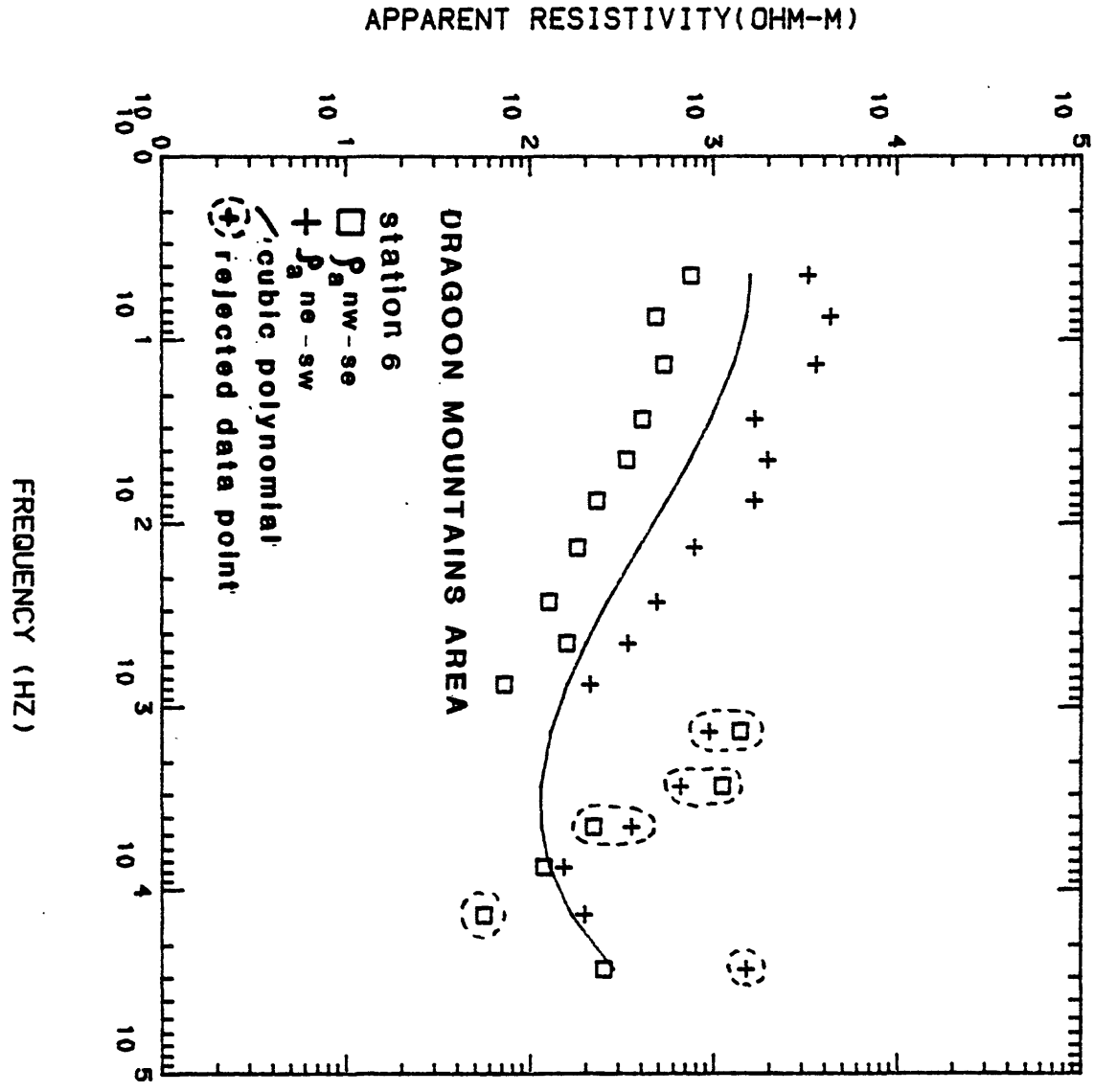
APPARENT RESISTIVITY(OHM-M)
DRAGOON MOUNTAINS AREA
station 6
□ ρ_a nw-se
+ ρ_a ne-sw
cubic polynomial
rejected data point
FREQUENCY (HZ)

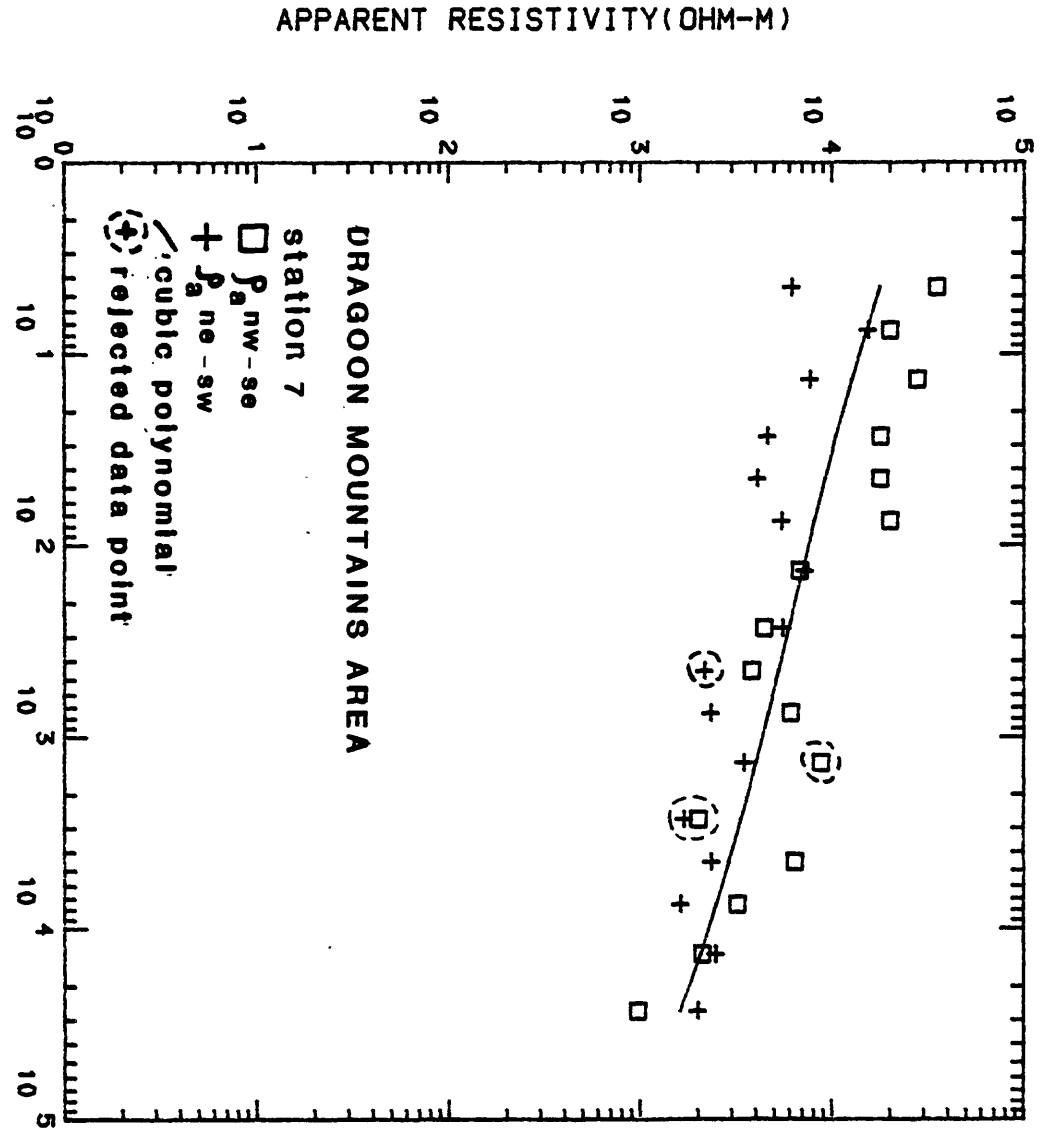
APPARENT RESISTIVITY(OHM-M)
DRAGOON MOUNTAINS AREA
station 7
□ ρ_a nw-se
+ ρ_a ne-sw
cubic polynomial
(+) rejected data point
FREQUENCY (HZ)

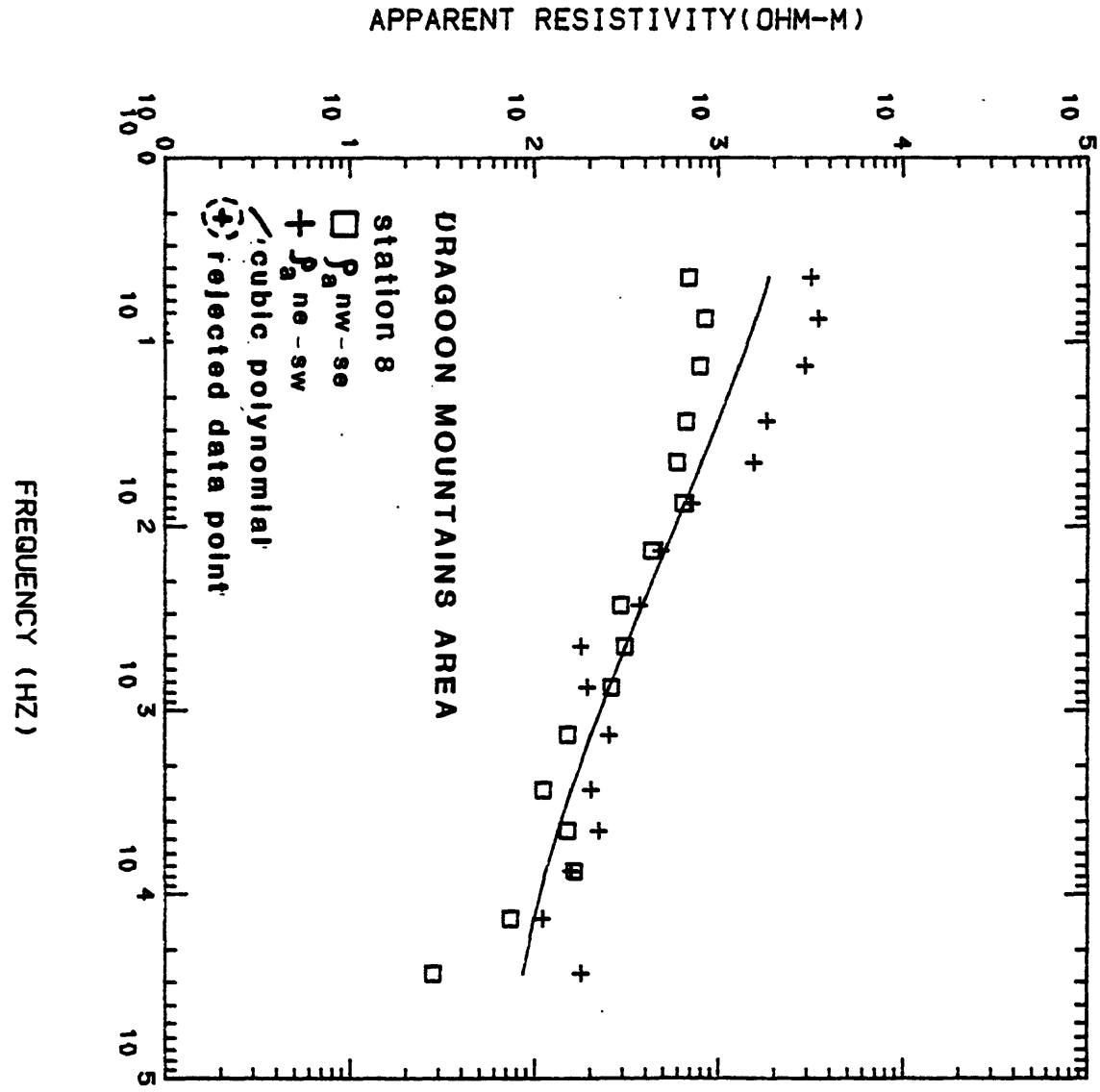
APPARENT RESISTIVITY(OHM-M)
FREQUENCY (HZ)
DRAGOON MOUNTAINS AREA
station 8
□ ρ_a nw-se
+ ρ_a ne-sw
cubic polynomial
(+) rejected data point

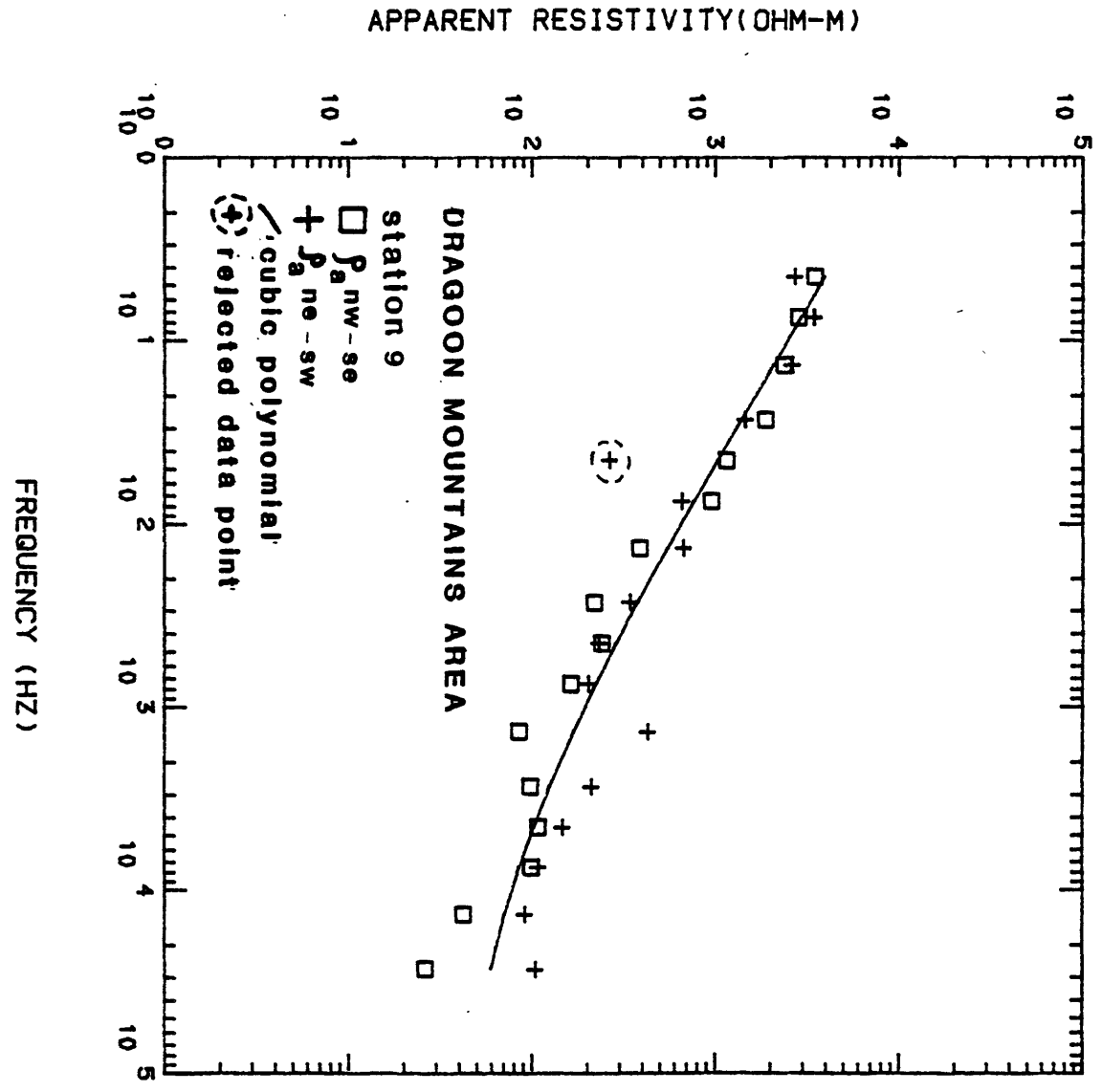
APPARENT RESISTIVITY(OHM-M)
FREQUENCY (HZ)
DRAGOON MOUNTAINS AREA
station 9
□ ρ_a nw-se
+ ρ_a ne-sw
\ cubic polynomial
(+) rejected data point

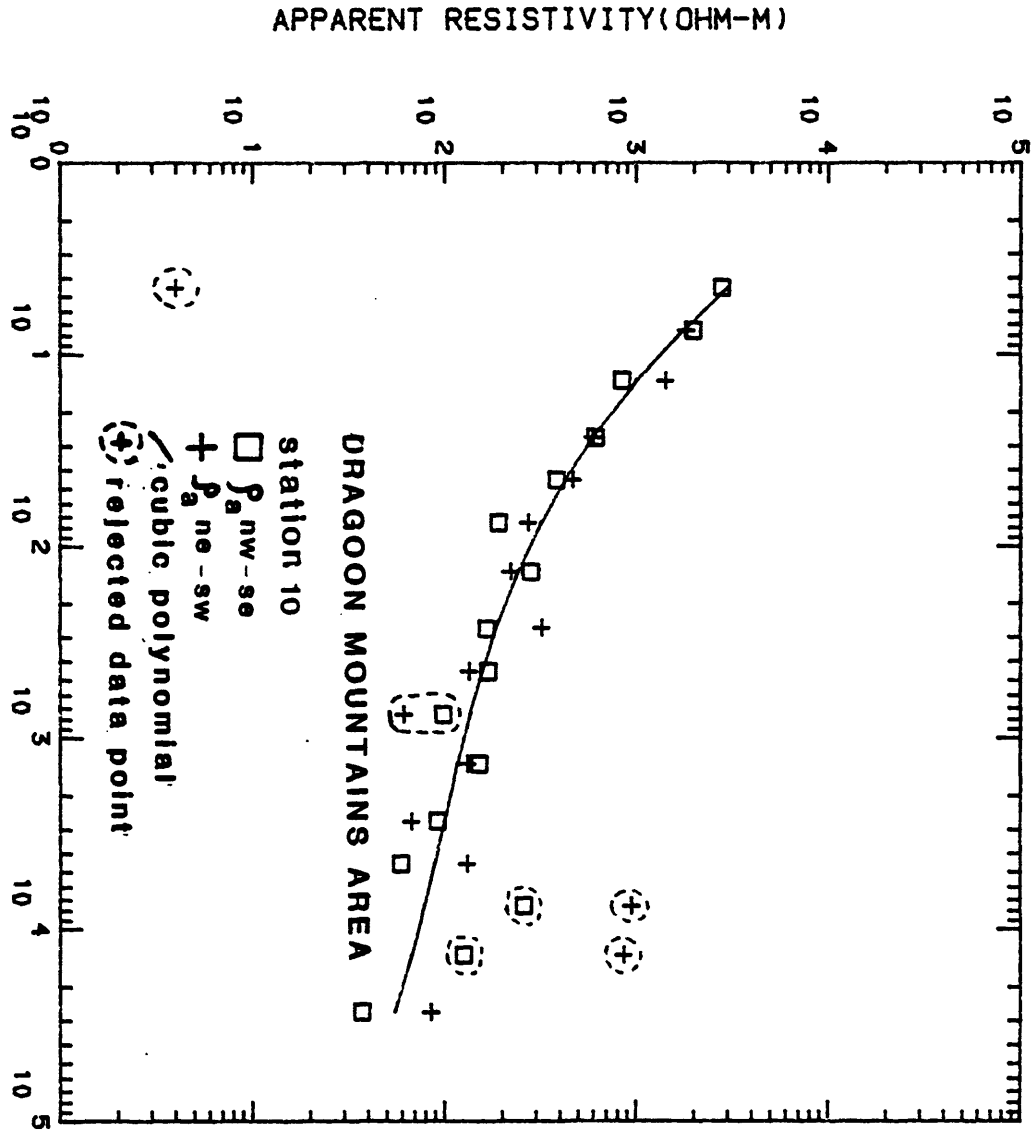
APPARENT RESISTIVITY(OHM-M)
FREQUENCY (HZ)
DRAGOON MOUNTAINS AREA
station 10
ρ_a nw-se
ρ_a ne-sw
cubic polynomial
rejected data point

Appendix C

Graphs of one-dimensional models of resistivity. Each bilogarithmic plot shows the resistivity-depth model (solid line) for each station along with the smoothed observed data (squares) and the forward solution (crosses) for the model presented. The observed data and the forward solution are plotted as apparent resistivity against apparent skin-depth. The starting model for each station was a layered equivalent to the Bostick transform of the bicubic polynomial approximation to the data (smoothed observed data) that is presented in Appendix B.

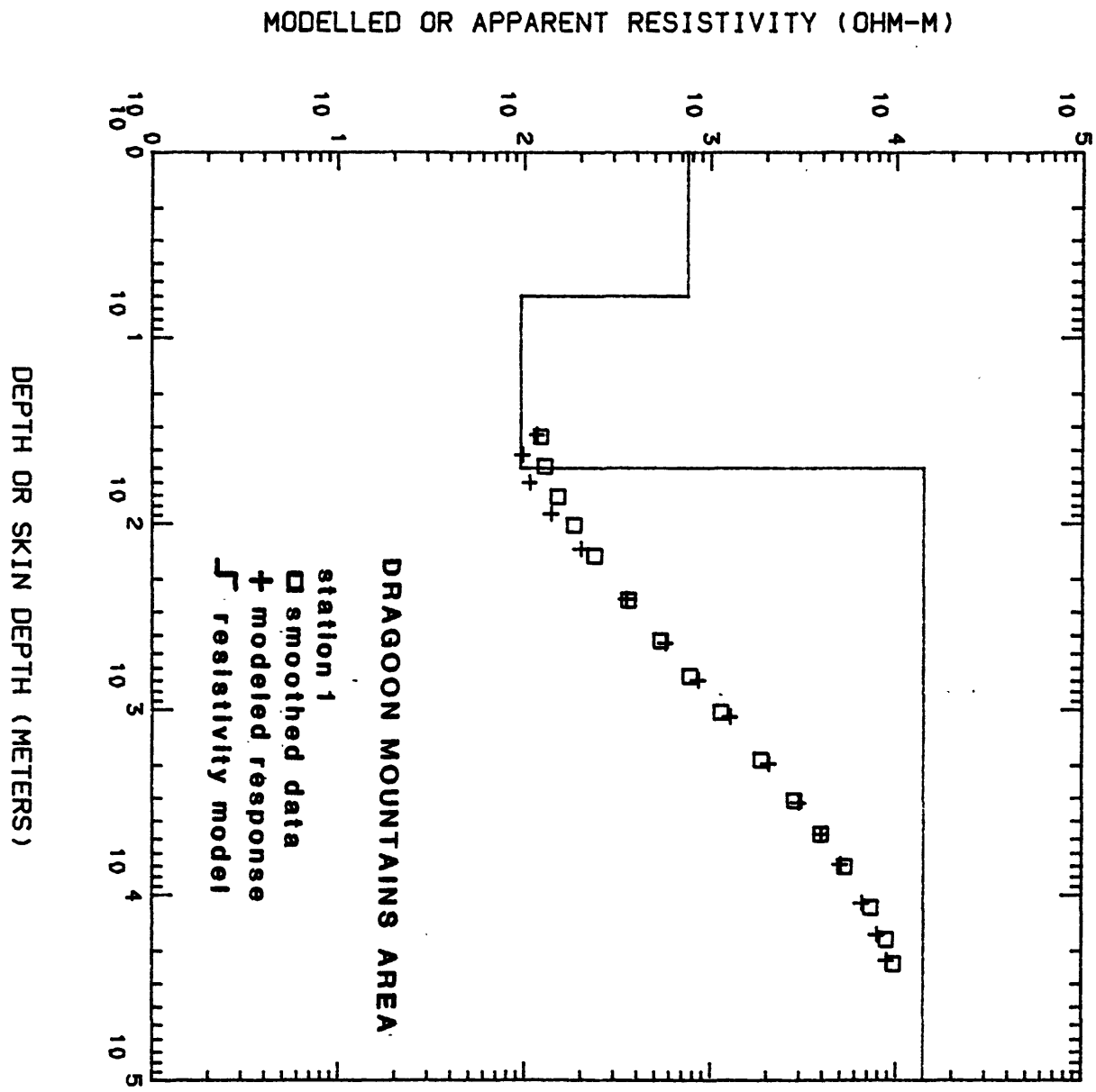
MODELLED OR APPARENT RESISTIVITY (OHM-M)
DEPTH OR SKIN DEPTH (METERS)
DRAGOON MOUNTAINS AREA
station 1
□ smoothed data
+ modeled response
resistivity model

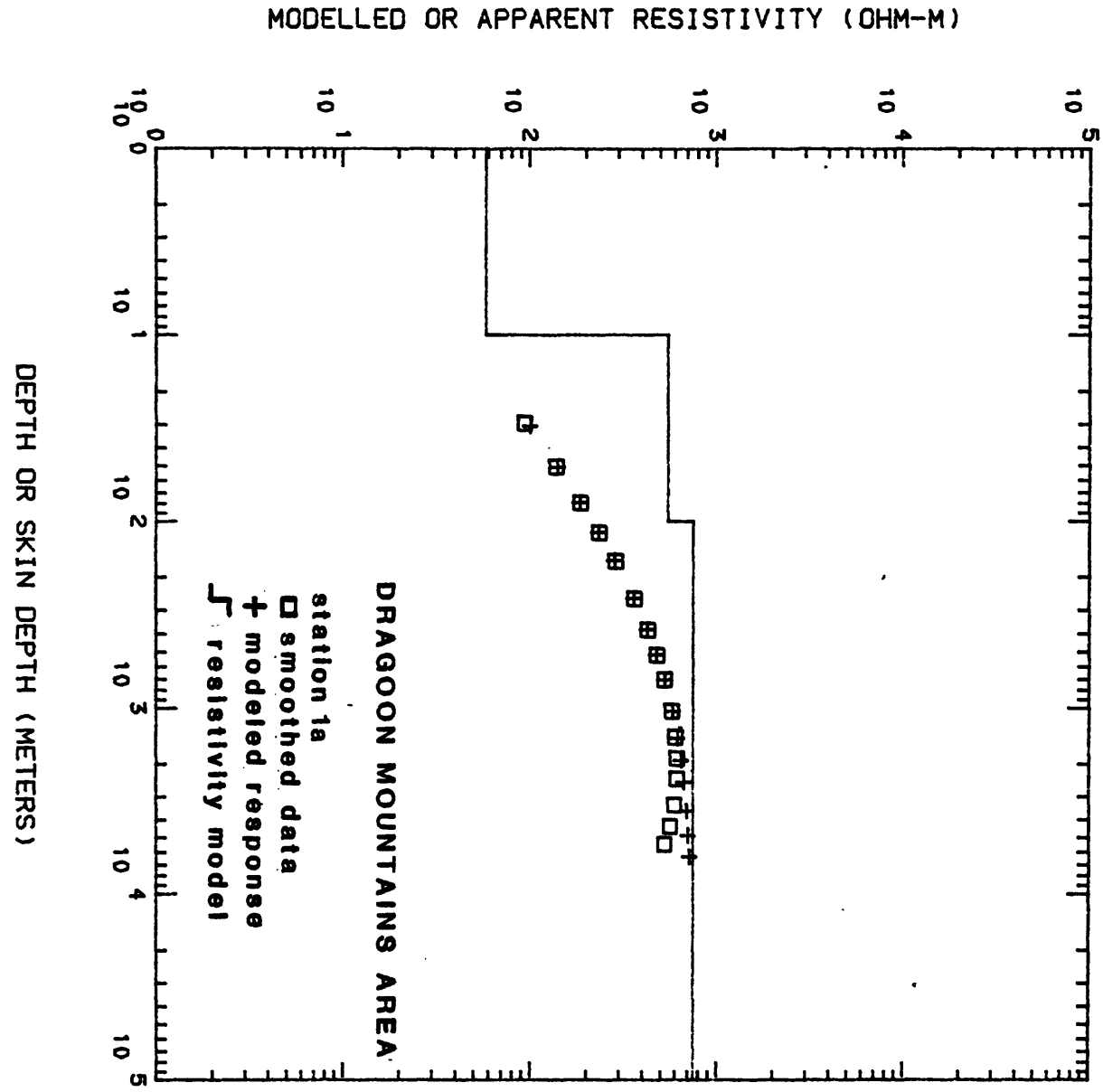
MODELLED OR APPARENT RESISTIVITY (OHM-M)
DEPTH OR SKIN DEPTH (METERS)
DRAGOON MOUNTAINS AREA
station 1a
smoothed data
modeled response
resistivity model

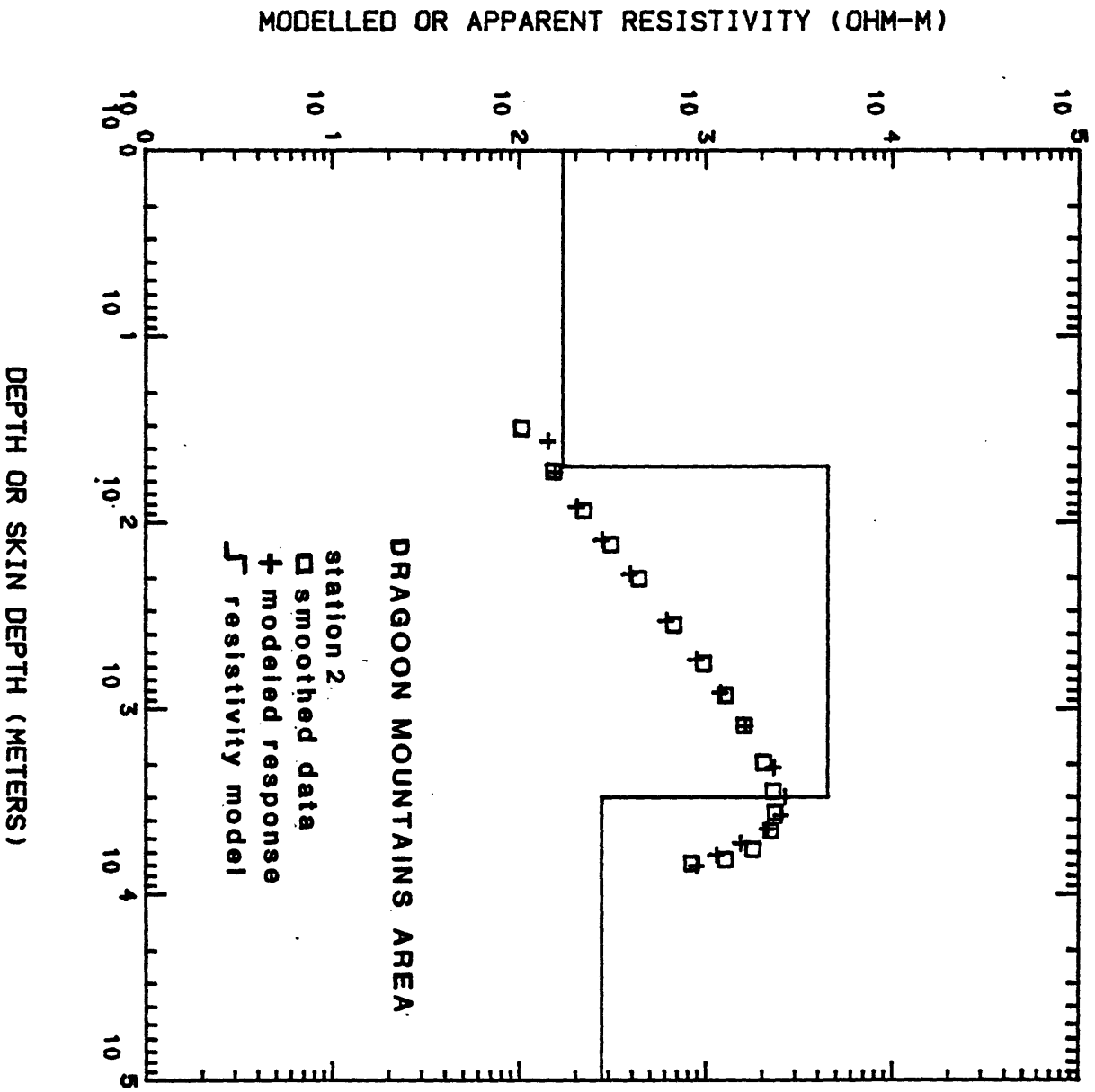
MODELLED OR APPARENT RESISTIVITY (OHM-M)
DEPTH OR SKIN DEPTH (METERS)
DRAGOON MOUNTAINS AREA
station 2
smoothed data
modeled response
resistivity model

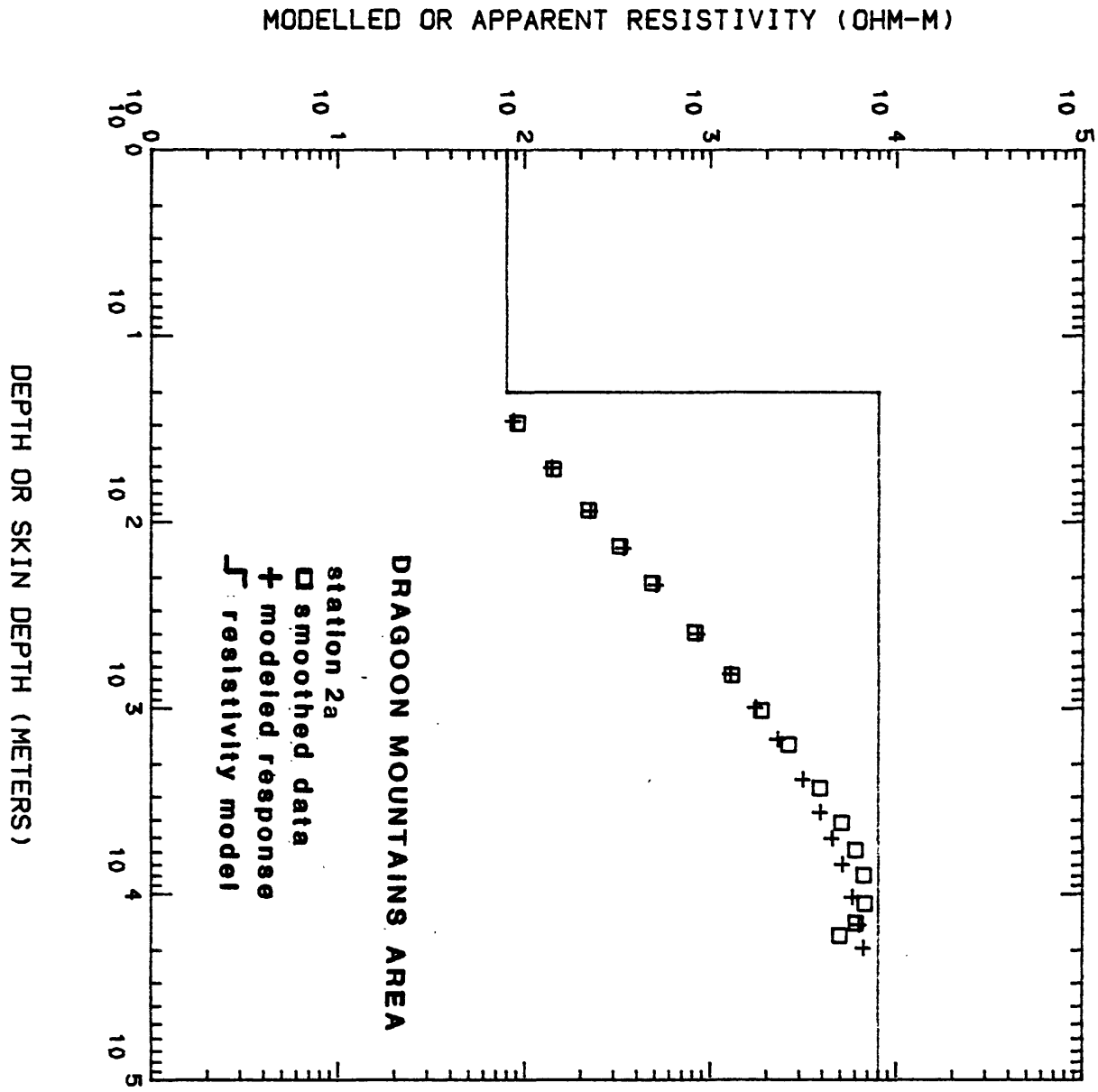
MODELLED OR APPARENT RESISTIVITY (OHM-M)
DEPTH OR SKIN DEPTH (METERS)
DRAGOON MOUNTAINS AREA
station 2a
smoothed data
modeled response
resistivity model

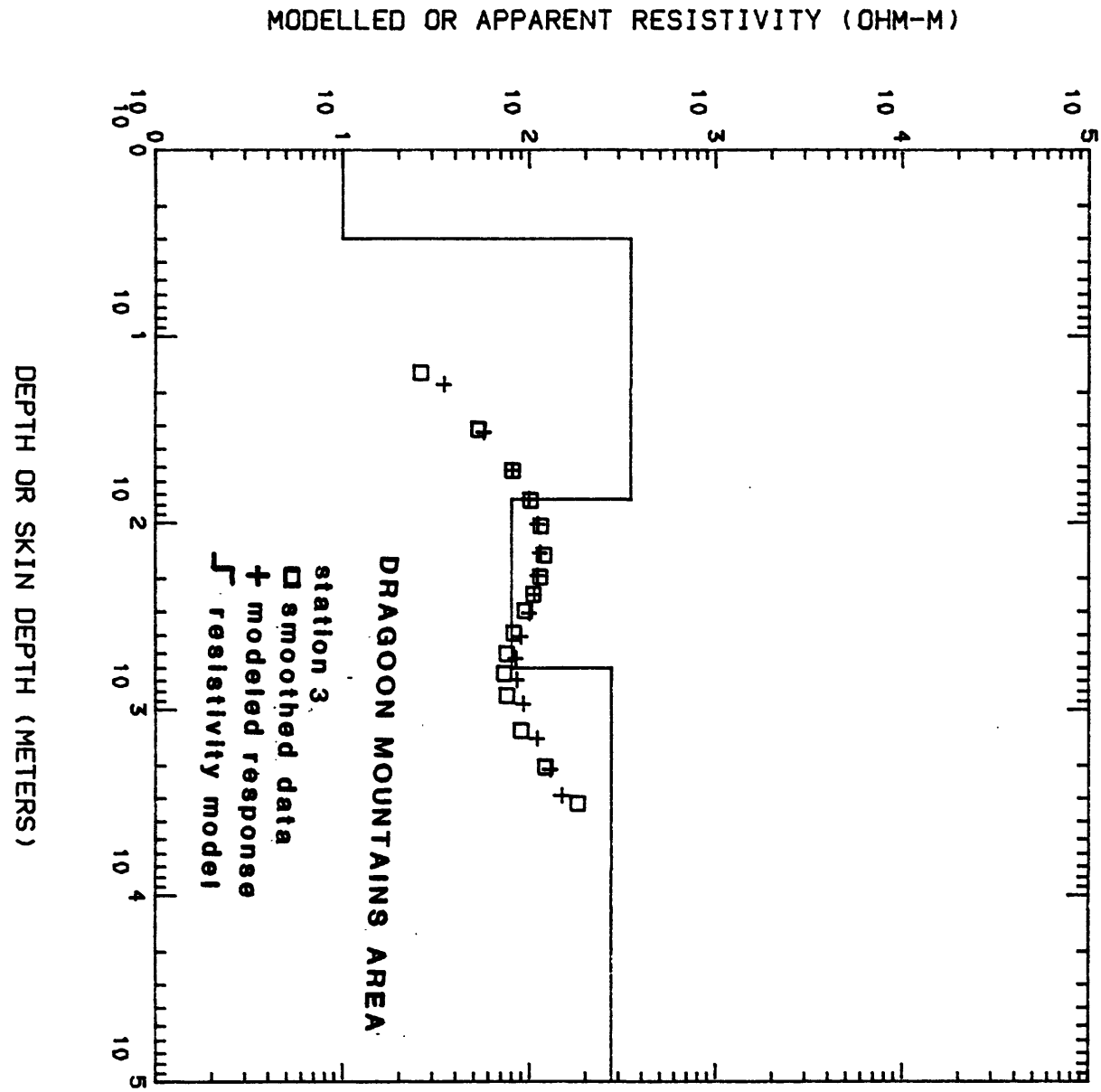
MODELLED OR APPARENT RESISTIVITY (OHM-M)
DEPTH OR SKIN DEPTH (METERS)
DRAGOON MOUNTAINS AREA
station 3
smoothed data
modeled response
resistivity model

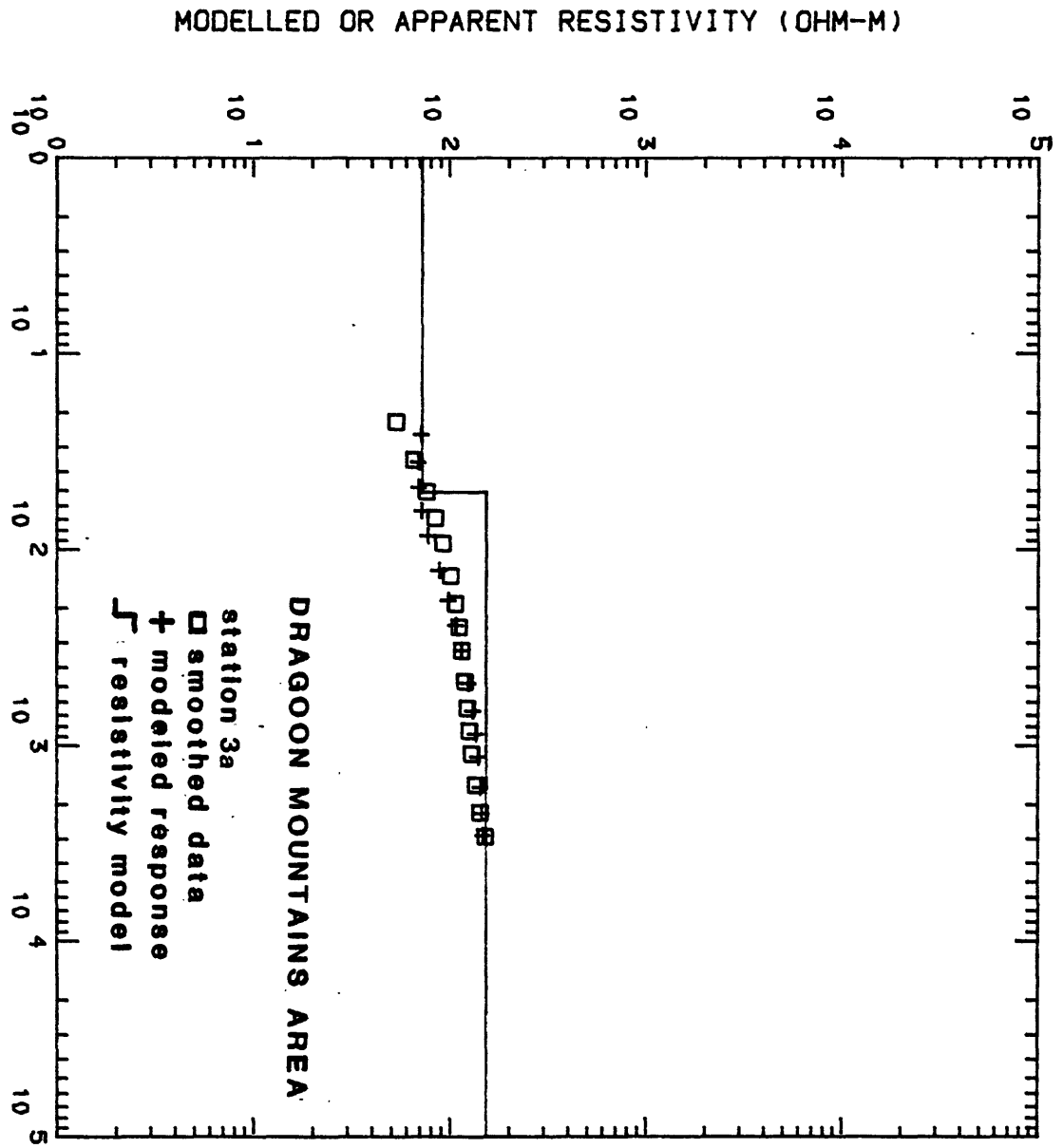
MODELLED OR APPARENT RESISTIVITY (OHM-M)
DEPTH OR SKIN DEPTH (METERS)
DRAGOON MOUNTAINS AREA
station 3a
smoothed data
modeled response
resistivity model

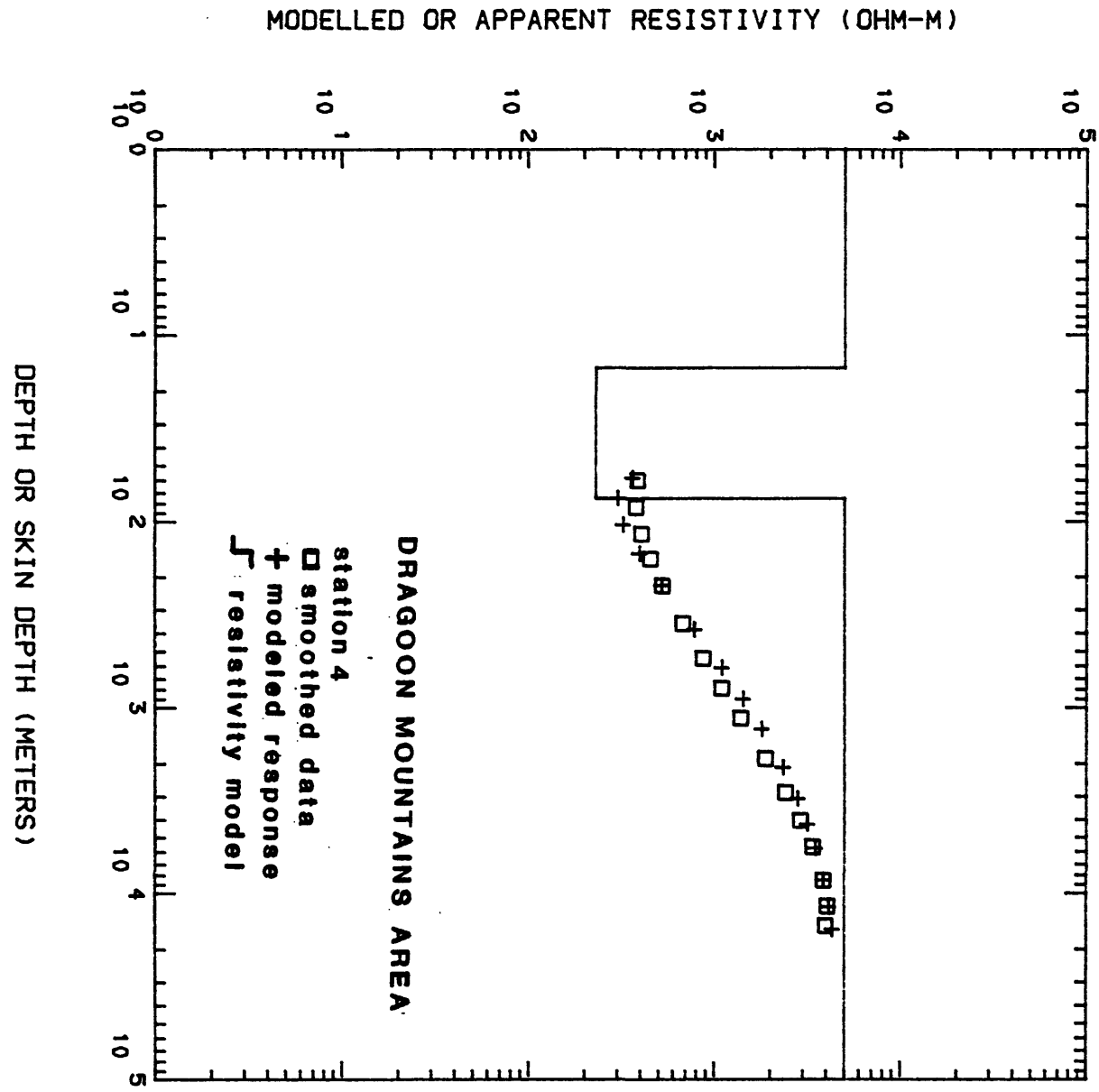
MODELLED OR APPARENT RESISTIVITY (OHM-M)
DEPTH OR SKIN DEPTH (METERS)
DRAGOON MOUNTAINS AREA
station 4
smoothed data
modeled response
resistivity model

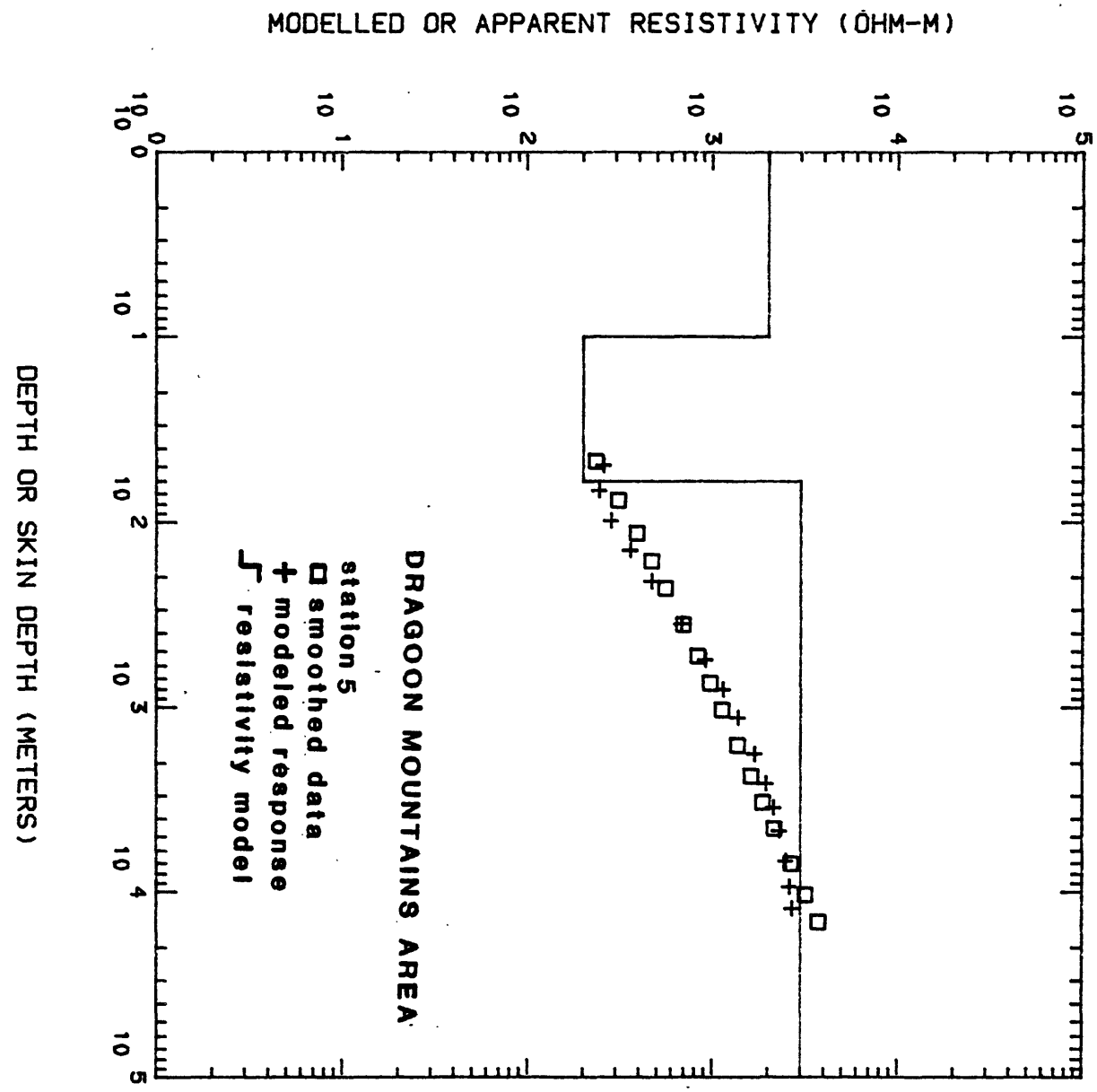
MODELLED OR APPARENT RESISTIVITY (OHM-M)
DEPTH OR SKIN DEPTH (METERS)
DRAGOON MOUNTAINS AREA
station 5
smoothed data
modeled response
resistivity model

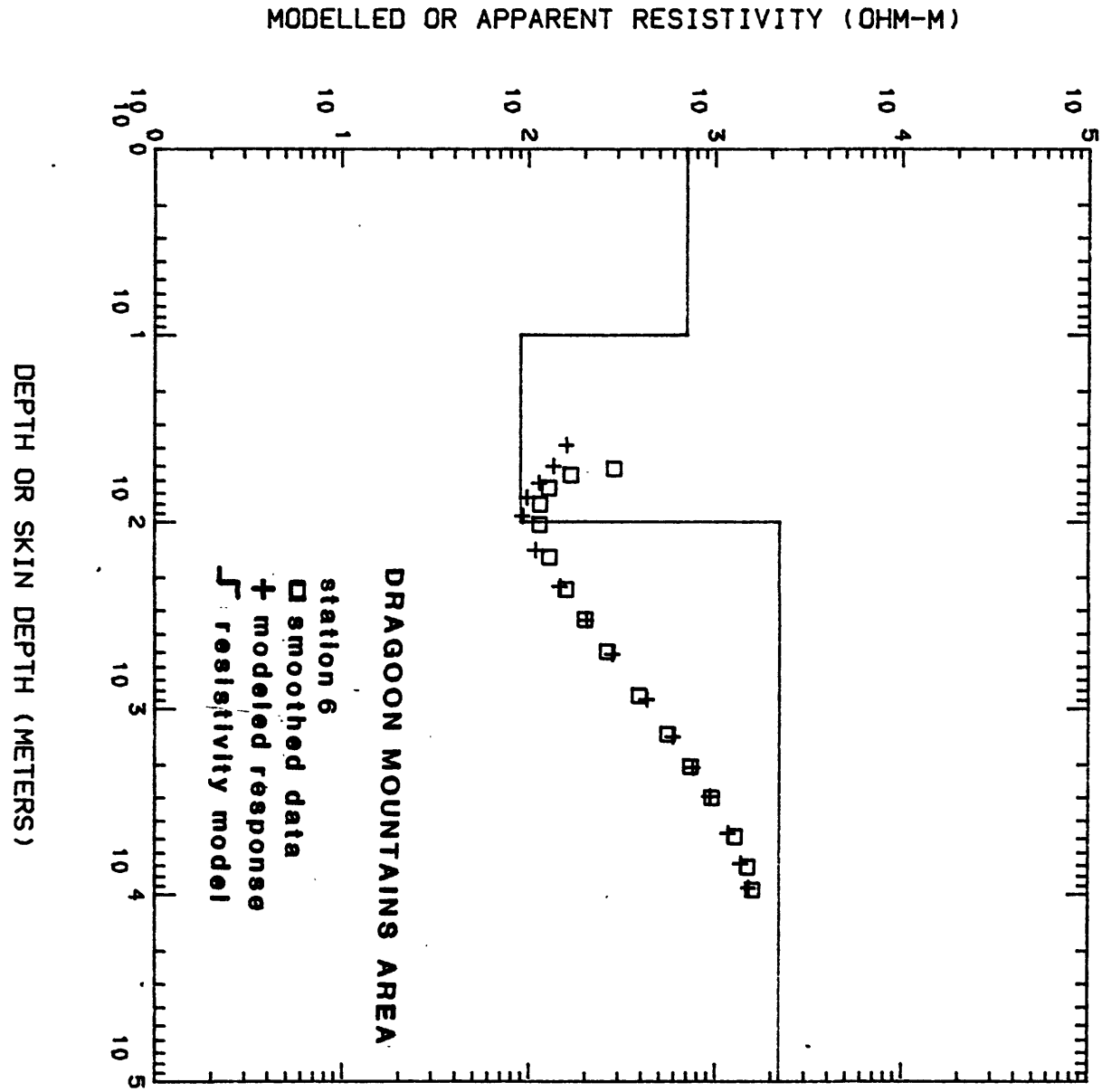
MODELLED OR APPARENT RESISTIVITY (OHM-M)
DEPTH OR SKIN DEPTH (METERS)
DRAGOON MOUNTAINS AREA
station 6
□ smoothed data
+ modeled response
resistivity model

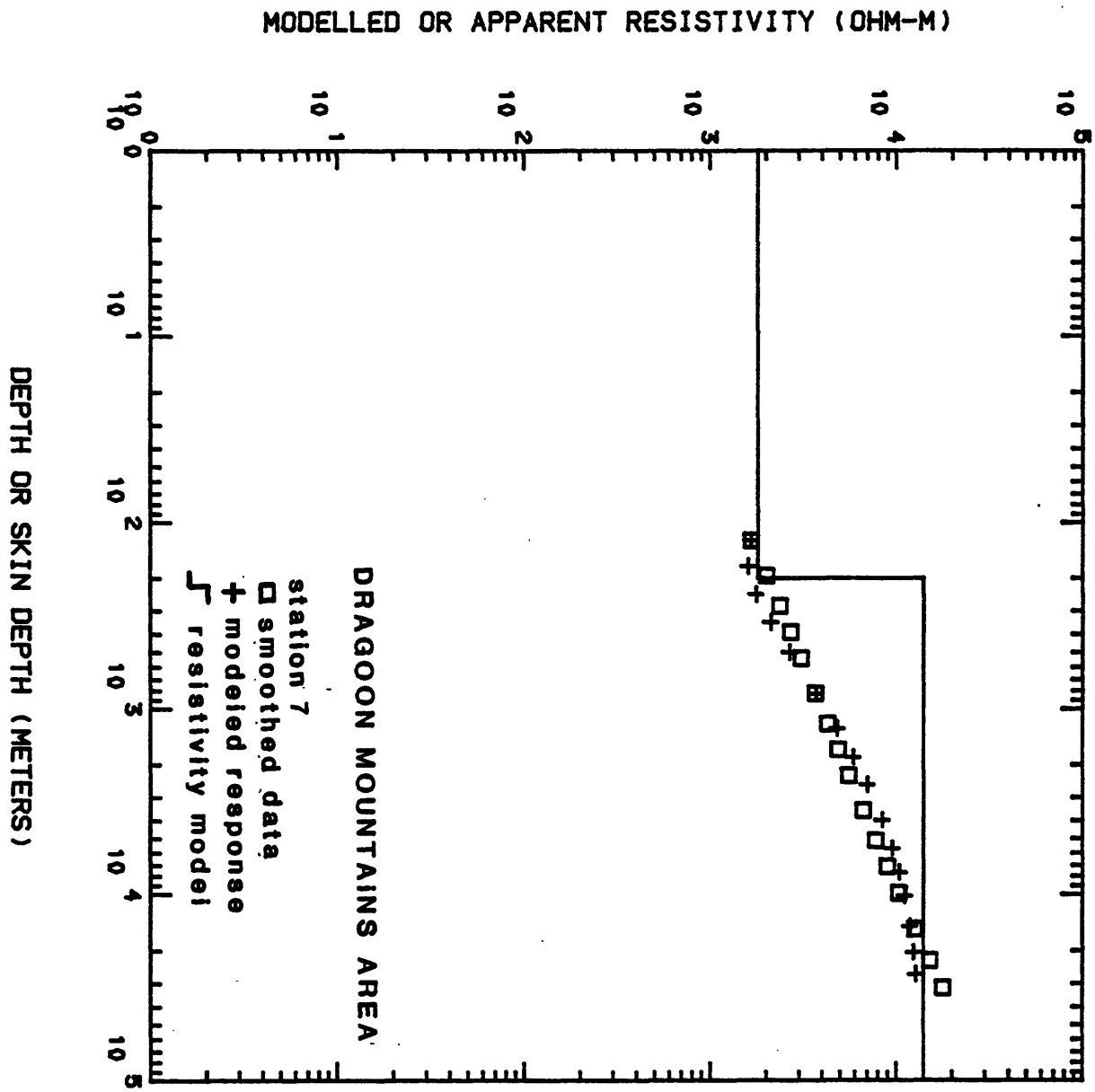
MODELLED OR APPARENT RESISTIVITY (OHM-M)
DEPTH OR SKIN DEPTH (METERS)
DRAGOON MOUNTAINS AREA
station 7
smoothed data
+ modeled response
resistivity model

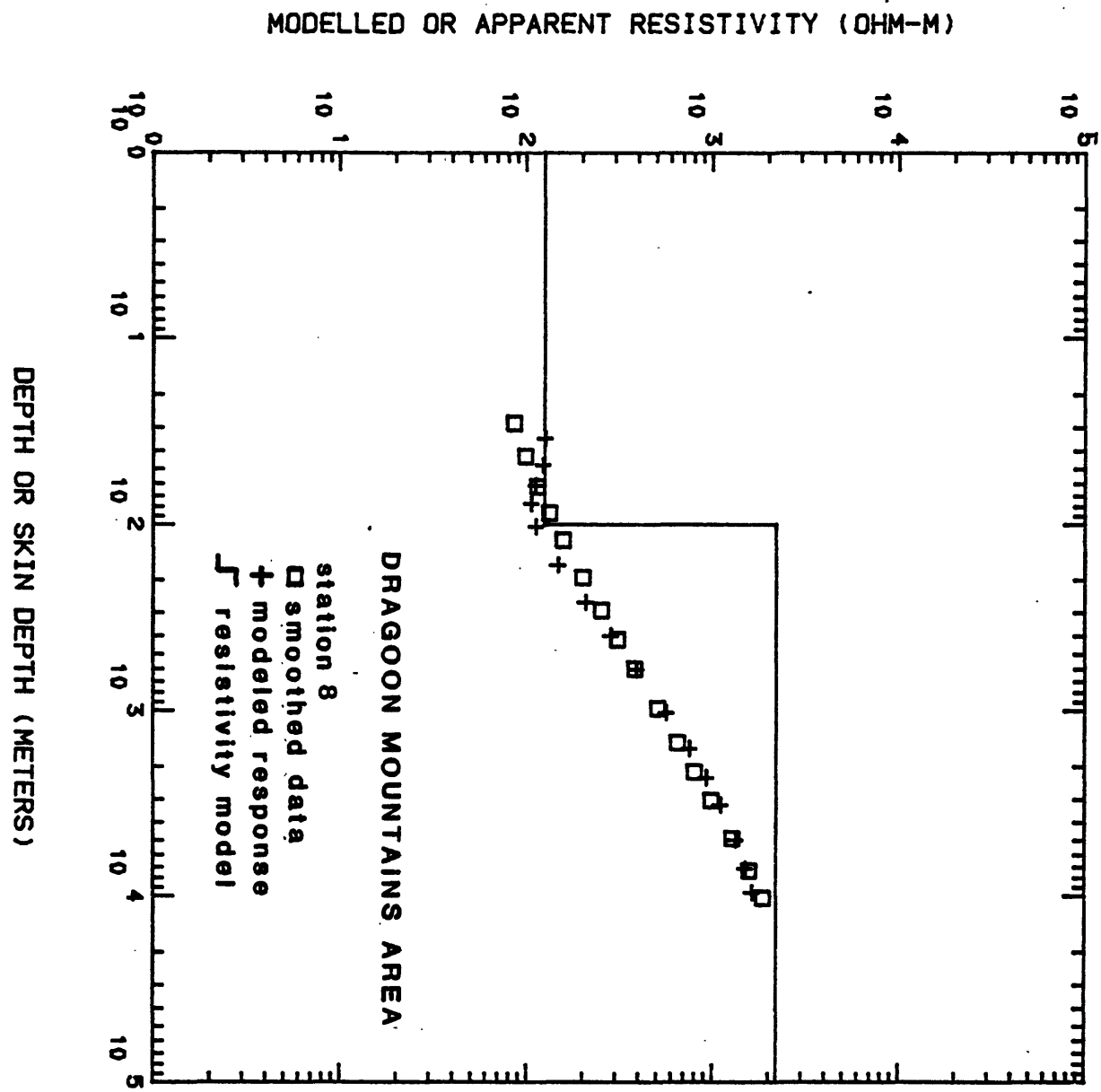
MODELLED OR APPARENT RESISTIVITY (OHM-M)
DEPTH OR SKIN DEPTH (METERS)
DRAGOON MOUNTAINS AREA
station 8
□ smoothed data
+ modeled response
resistivity model

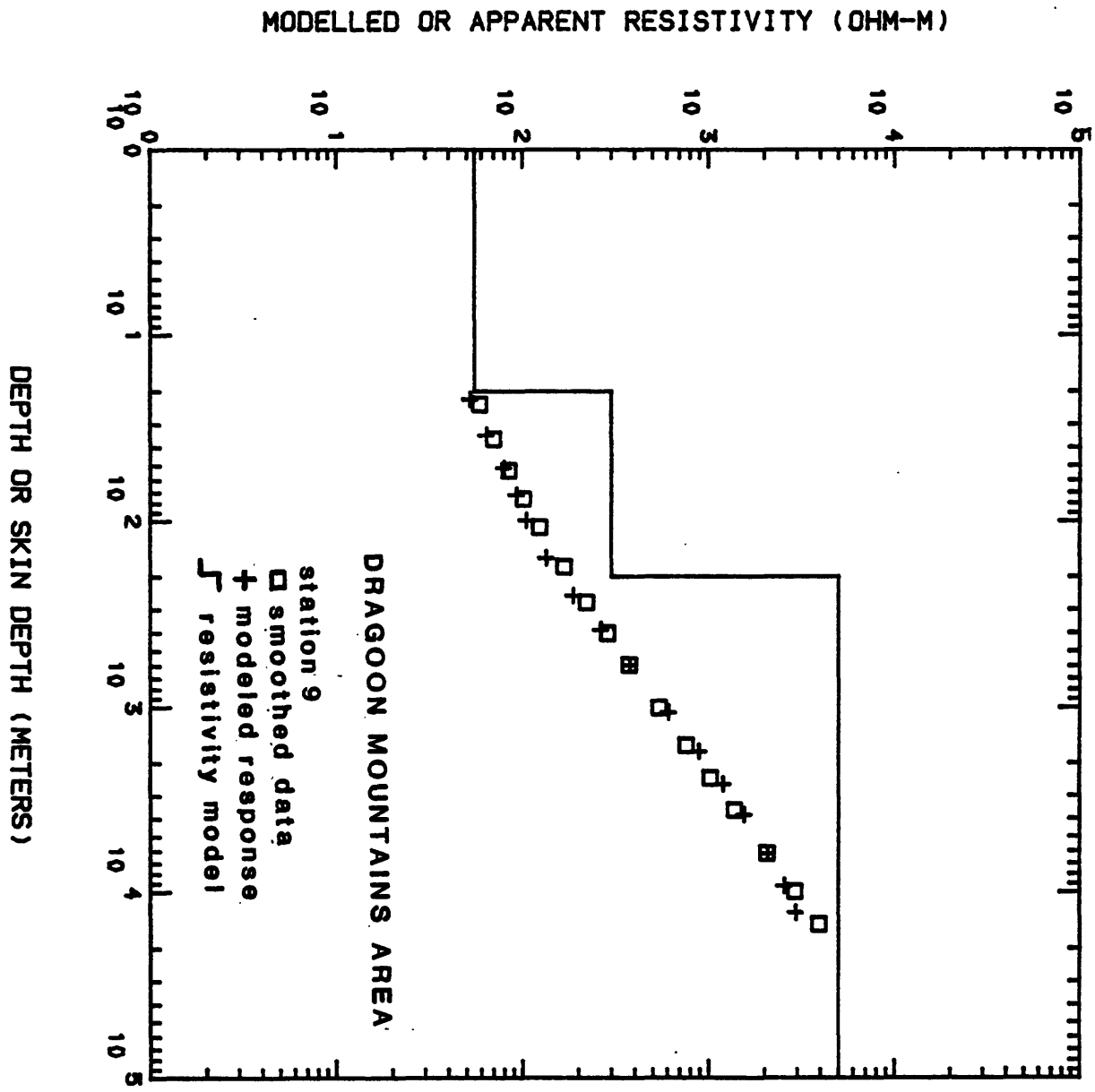
MODELLED OR APPARENT RESISTIVITY (OHM-M)
DEPTH OR SKIN DEPTH (METERS)
DRAGOON MOUNTAINS AREA
station 9
□ smoothed data
+ modeled response
resistivity model

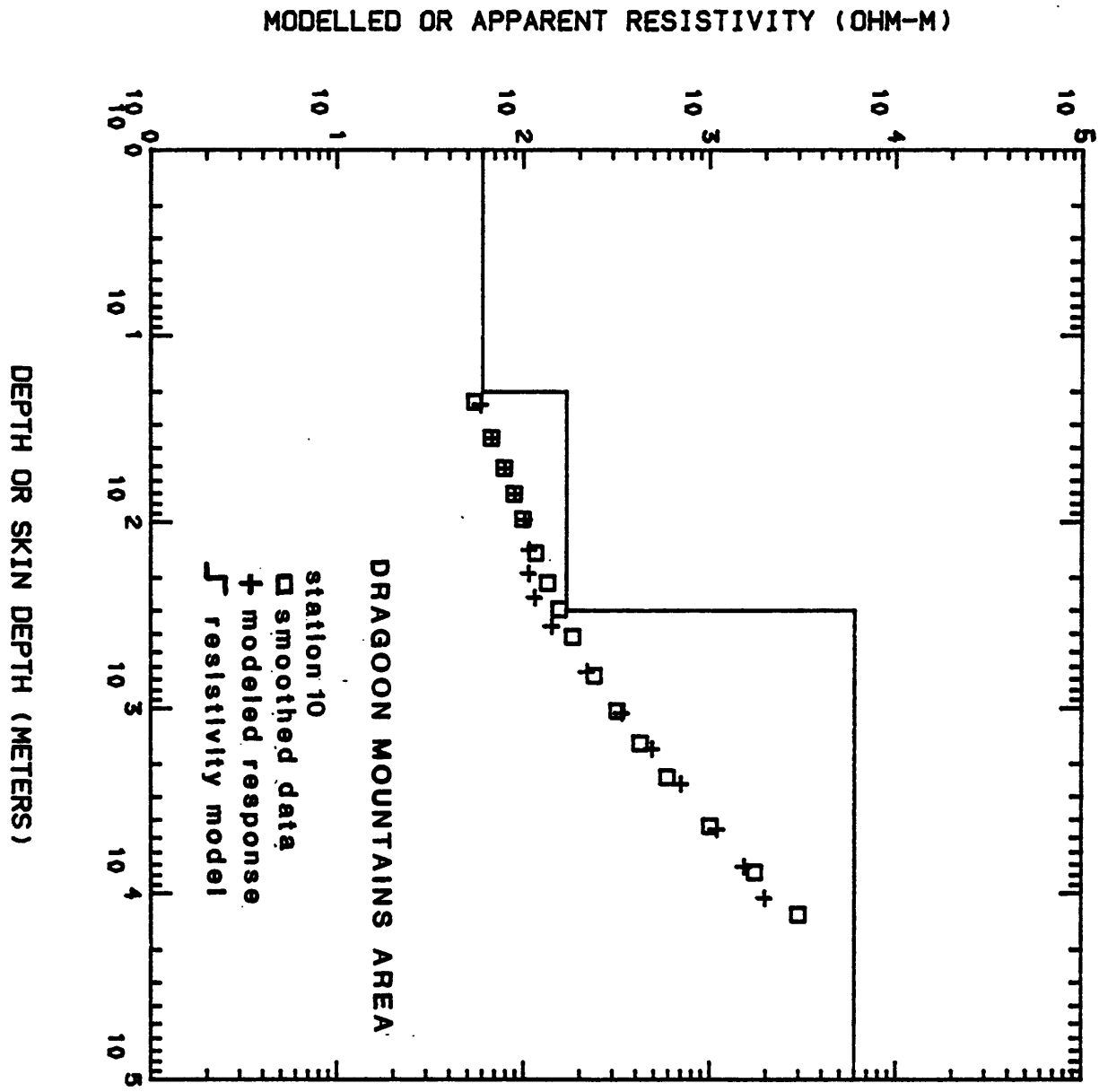
MODELLED OR APPARENT RESISTIVITY (OHM-M)
DEPTH OR SKIN DEPTH (METERS)
DRAGOON MOUNTAINS AREA
station 10
□ smoothed data
+ modeled response
resistivity model